A Novel Robotic Platform for Aerial Manipulation using Quadrotors as Rotating Thrust Generators

Hai-Nguyen Nguyen, Sangyul Park, Junyoung Park and Dongjun Lee

***Abstract*—We propose a novel robotic platform for aerial operation and manipulation, *SmQ (spherically-connected multi-quadrotor)* platform, which consists of a rigid frame and multiple quadrotors, that are connected to the frame via passive spherical joints and act as distributed rotating thrust generators to collectively propel the frame by adjusting their attitude and thrust force. Depending on the number of quadrotors and their configuration, this SmQ platform can fully (or partially) overcome the issues of under-actuation of the standard multi-rotor drones for aerial operation/manipulation (e.g., body-tilting with side-way gust/force, dynamic interaction hard to attain, complicated arm-drone integration, etc.). We present the dynamics modeling of this SmQ platform system and establish the condition for its full-actuation in SE(3). We also show how to address limited range of spherical joints and rotor saturations as a constrained optimization problem by noticing the similarity with multi-fingered grasping problem under friction-cone constraint. We then design and analyze feedback control laws for the S3Q and S2Q systems as a combination of high-level Lyapunov control design and low-level constrained optimization; and show that the (fully-actuated) S3Q system can assume any trajectory in SE(3), whereas the S2Q system in $\Re^3 \times \mathbf{S}^2$ with its un-actuated dynamics still internally stable. Experiments are also performed to show the efficacy of the theory.**

I. Introduction

Multi-rotor drones (e.g., quadrotor, hexarotor, octarotor, etc.) have received considerable attention from research communities and general public alike due to their potentials in a wide range of applications. The rapid developments in sensors (e.g., MEMS (micro-electromechanical system) IMU (inertial measurement unit), GNSS (global navigation satellite system), camera), motors (e.g., BLDC (brush-less direct current) motors), batteries (e.g., LiPo (lithium-polymer) battery), materials (e.g., carbon fiber), onboard computing and wireless communication technologies, spurred by consumer electronics and IT (information technology) industry, have substantially lowered the price of the multi-rotor drones, even with many now affordable to general customers, hobbyists, etc. At the same time, the fast advancements in sensor fusion, SLAM (simultaneous localization and mapping), computer vision and control technologies have enabled many successful applications for the multi-rotor drones, with aerial photography, geo-survey, traffic monitoring, pesticide spraying, surveillance and reconnaissance as the most representative ones. Despite this, as also can be seen just above, the successful applications of the multi-rotor drones have been mostly limited to *passive observation*, and it is deemed by many groups and companies that the potential of the multi-rotor drones for *physical interaction* (e.g., aerial operation/manipulation) should be tapped not only for academic research but also to drastically expand the commercial market of the multi-rotor drones.

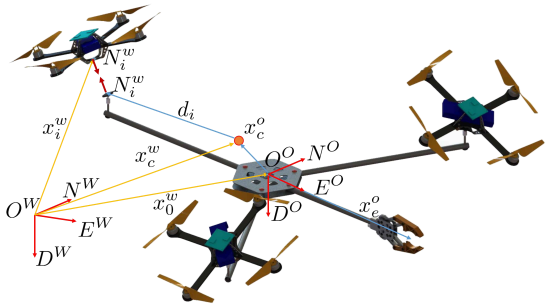

Fig. 1: Spherically-connected multi-quadrotor (SmQ, with $m = 3$) platform, consisting of multiple quadrotors connected to a rigid frame (or tool) via passive spherical joints.

The key challenge in using the multi-rotor drones for aerial operation/manipulation is their *under-actuation*, i.e., with all the rotors colinearly attached to the body, it cannot change the forcing (or thrust) direction without tilting the platform itself. To better see this, consider the drone-manipulator systems (i.e., multi-rotor drone with multi-DOF (degree-of-freedom) robotic arm), which, although most-widely studied for aerial manipulation (e.g., [1], [2], [3], [4], [5], [6], [7], [8], [9]), possess the following limitations due to its under-actuation coupled with the current limited motor technology[1]: 1) they typically cannot push side-way or resist lateral gust without tilting its body (e.g., difficult to maintain operation/manipulation contact) as their majority is equipped with a robot arm only with small-DOF (e.g., two-DOF [1], [2], [6], [8], [9]); 2) they typically cannot attain "dynamic" (i.e., fast/smooth) interaction control, as their majority is equipped not with a torque-controlled robot arm (e.g., [1], [2], [8], [9]) and such dynamic interaction may destabilize the un-actuated dynamics; and 3) their arm-drone integration and control synthesis are typically fairly complicated, since the issue of under-actuation (e.g.,

Submitted to the IEEE Transactions on Robotics, November 2016. Revised and Resubmitted November 2017. Accepted December 2017. Paper Type: Regular Paper.

The authors are with the Department of Mechanical & Aerospace Engineering and IAMD, Seoul National University, Seoul, Republic of Korea, 08826. Email: {hainguyen,sangyul,sunny9298,djlee}@snu.ac.kr

Corresponding author: Dongjun Lee.

This research was supported by Basic Science Research Program (2015R1A2A1A15055616) of the National Research Foundation (NRF) of Korea funded by the Ministry of Science & ICT (MSIT); and the Industrial Strategic Technology Development Program (10060070) of the Ministry of Trade, industry & Energy (MOTIE) of Korea.

[1]See Sec. I-A for comparison with other types of aerial manipulation systems.

instability) can only be properly addressed by considering their full dynamics. This we believe is because the multi-rotor drones are optimized for the ease of flying (e.g., for hobbyists), but not necessarily for other applications such as aerial operation/manipulation.

In this paper, we propose a novel robotic platform for aerial operation and manipulation, namely, **SmQ (spherically-connected multi-quadrotor)** platform - see Fig. 1. This SmQ platform consists of a rigid frame (or tool) and multiple quadrotors (or multi-rotor drones), which are connected to the frame via passive spherical joints. Each of these quadrotors is then used as the actuator for the frame, that is, by controlling its attitude and thrust force, they can collectively produce the motion of the frame in SE(3). In other words, we use the quadrotors as distributed rotating thrust generators. Depending on the number of quadrotors and their configuration, this SmQ platform can fully (e.g., S3Q platform of Sec. IV) or partially (e.g., S2Q platform of Sec. V) overcome the aforementioned issues of under-actuation of the multi-rotor drones. Adopting multiple quadrotors, this SmQ platform often possesses larger payload than a single multi-drone system. This SmQ platform may be used as a stand-alone aerial tool system with some end-effector (e.g., drill, driver, etc.) attached to it (e.g., Sec. VI); or as a platform for a multi-DOF robotic arm for dexterous aerial manipulation, for which the platform-arm integration can be simple and even "modular" (e.g., combination of SmQ platform and robot arm impedance controls; or even their kinematic controls combination), as the (fully-actuated) SmQ system is kinematically-reducible [10]. Note also that this SmQ platform can be quickly constructed by using off-the-shelf/commercial multi-rotor drones, which are often shipped with well-functioning low-level attitude/thrust controls.

The main goal of this paper is to provide theoretical framework for this SmQ platform system, particularly, for its modeling and control. Experimental validation is also performed. Motion planning is briefly touched as well, yet, spared for future research, since, due to its peculiarity (i.e., dependency among control inputs), it cannot be addressed in a standard manner. We first provide the dynamics modeling of this SmQ platform and establish the geometric condition for their full-actuation in SE(3). We also show how to address the issue of limited range of (commercial) spherical joints and the rotor saturations - the key technical challenge of the SmQ platform systems - as a constrained optimization problem by noticing its similarity with the well-known multi-fingered grasping problem under the friction-cone constraint [11]. We then design and analyze control laws for the (fully-actuated) S3Q system and for the (partially-actuated) S2Q system as a combination of high-level Lyapunov control design (to achieve trajectory tracking) and low-level constrained optimization (to comply with the physical limited-range/thrust constraints); and show that the S3Q system can attain the trajectory tracking in SE(3), whereas the S2Q system in $\Re^3 \times S^2$ with its un-actuated dynamics still internally stable in practice. We then perform the experiments for prototype S3Q and S2Q platform systems to validate these theoretical results and demonstrate their performance.

A. Comparison with Other Aerial Manipulation Systems

In contrast to the drone-manipulator system (e.g., [1], [2], [3], [4], [5], [6], [7], [8], [9]) with some of its limitations as stated above, our SmQ platform can: 1) resist side-way gust/force while holding its attitude due to its full-actuation in SE(3); 2) attain "dynamic" interaction control with its full-actuation and force/torque-level actuation; and 3) integrate with a robotic arm in a "modular" manner (e.g., simply combine impedance controls of arm and platform; or even their kinematic-level control), again due to its full-actuation. Of course, our SmQ platform is not without its shortcomings and perhaps the most significant one would be its large form-factor due to its requiring additional quadrotors. This large form-factor may be detrimental (or even not allowable) for some applications, for which the drone-manipulator system or other aerial manipulation systems as stated below would be preferred.

The issue of under-actuation has been recognized by many researchers and some of them, including us, have proposed *tilted multi-rotor platforms* (e.g., [12], [13], [14], [15], [16]), where multiple rotors are asymmetrically attached to the body to directly produce full-actuation in SE(3), with some of them capable of even such challenging behaviors as 360^o pitch-turning and large-force downward pushing (e.g., [15], [16]), all impossible with our SmQ platform system. This tilted multi-rotor platform is also generally of smaller form-factor than the SmQ platform. However, due to the inter-rotor flow interference, necessarily arising from the rotors not colinear with each other, energy efficiency, and, consequently, flight time of this tilted multi-rotor platform is rather limited.

Another system along this line is *tilting multi-rotor platform*, where the tilting angles of the rotors of a multi-rotor drone are actively controlled with extra actuators via some tilting mechanisms (e.g., [17], [18], [19], [20]). This tilting multi-rotor platform can then overcome the issue of under-actuation as our SmQ platform does with its form-factor again typically smaller than the SmQ system. However, addition of these extra actuators and mechanisms may significantly reduce (often already fairly tight) payload/flight-time, and, further, substantially increase system complexity (and, consequently, maintenance difficulty and reliability), losing the very advantage of the multi-rotor platform (as compared to, e.g., helicopter platform with the complex swash plate mechanism).

Yet another way for aerial operation/manipulation is to utilize multiple quadrotors. For this, the authors of [21], [22] rigidly attach multiple quadrotors essentially to a frame to increase loading capability of the system. However, with all the rotors again colinear, these platforms are again under the same limitations stemming from the under-actuation. On the other hand, cable-suspended systems using multiple quadrotors are presented in [23], [24], [25], which, yet, we believe, would be not so suitable for many aerial operation/manipulation applications, as they cannot control the swaying motion of the object in the presence of gusts.

Portions of this paper were presented in [26]. In this paper, we generalize and complete the results in our previous work. We first expand the control design for general pose tracking for

both S2Q-platform and S3Q-platform with the proof of their effectiveness. We relax the assumption on the symmetry of the S2Q system, and present the derivation and analysis of the internal dynamics of S2Q-platform here for the first time. We also provide a complete treatment for the problem of optimal control allocation with the analysis of solution existence and a real-time solver. New experiments are also performed to illustrate the capabilities of the proposed platform.

The rest of this paper is organized as follows. The design and dynamical model of the system are presented in Sec. II. The actuation capacity and the control feasibility of the system are analyzed in Sec. III. The control design and optimal control allocation for motion control of the system with three quadrotors and that with only two quadrotors are presented in Sec. IV and Sec. V, respectively. In Sec. VI we present experimental results and discussions. Some concluding remarks are given in Sec. VII.

II. System Design and Modeling

A. System Description

Consider the *SmQ (spherically-connected multi-quadrotor)* platform system with m ($m = 1, 2, ..., n$) being the number of quadrotors attached to the frame as shown in Fig. 1. We design the joint-quadrotor connection in such a way that each spherical joint is attached at the center-of-mass of the quadrotors as close as possible. Some offset inevitably arises from this connection design, which yet appears to be effectively suppressed by the feedback control as demonstrated in Sec. VI. We then have the following relation between the center-of-mass position[2] $x_i^w \in \Re^3$ of the i-th quadrotor and that of the SmQ-frame $x_o^w \in \Re^3$, all expressed in the inertial frame $\{\mathcal{F}_W\}$ s.t.,

$$x_i^w = x_o^w + R_o x_i^o, \quad i = 1, 2, ..., n \tag{1}$$

where $x_i^o \in \Re^3$ is x_i expressed in the body frame $\{\mathcal{F}_0\}$ fixed to the center-of-mass of the SmQ-frame, and $R_o \in$ SO(3) is the attitude of the frame expressed in $\{\mathcal{F}_W\}$. See Fig. 1, where we use the north-east-down convention to represent each frame.

We can then assume that each quadrotor can rotate about the passive spherical joint with its rotation dynamics (w.r.t. center-of-mass) decoupled from that of the SmQ-frame, while generating the thrust force vector $\Lambda_i^o := \lambda_i R_o^T R_i e_3 \in \Re^3$ and exerting the constraint force $N_i^w \in \Re^3$ on the SmQ-frame through the attaching point $x_i \in \Re^3$ to enforce the constraint (1). Here, $\lambda_i > 0$ and $R_i \in$ SO(3) are respectively the thrust force magnitude and the attitude of the i-th quadrotor expressed in $\{\mathcal{F}_W\}$. No reaction moment is transmitted from the quadrotor to the SmQ platform via the passive spherical joint.

Real spherical joints only allow for limited range of motion, typically smaller than $(-35°, +35°)$ in pitch and roll directions, although the yaw motion can be unconstrained. This limited motion range of the spherical joints can be modeled by the following cone constraint:

$$(p_i^o)^T \Lambda_i^o \geq \|\Lambda_i^o\| \cos\phi_i, \quad i = 1, 2, ..., n \tag{2}$$

where $p_i^o \in \Re^3$ is the unit vector along the direction of the center axis of the i-th spherical joint, $\phi_i \in \Re$, $0 < \phi_i < \pi/2$, is its maximum range of angle motion, and $\|\Lambda_i^o\| := \sqrt{(\Lambda_i^o)^T \Lambda_i^o} \geq 0$, which is also in general bounded, i.e., there exists $\bar{\lambda}_i \geq 0$ s.t., $||\Lambda_i^o|| < \bar{\lambda}_i$, $i = 1, 2, ..., n$. See Fig 2. Note that this joint constraint (2) with $\phi_i < \pi/2$ also implies the quadrotor thrust λ_i always be positive. The design, control, and analysis of the SmQ platform system should then fully incorporate this range constraint of the spherical joints and also the limited actuation of thrust generation - see Sec. III, Sec. V and Sec. IV.

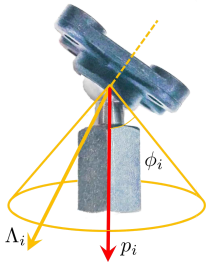

Fig. 2: Range limit of spherical joint: $p_i \in \Re^3$ is the center-axis unit vector, ϕ_i the maximum allowable motion range, and $\Lambda_i \in \Re^3$ the quadrotor thrust vector.

B. Dynamics Modeling and Reduced Dynamics

With the assumption that the spherical joint is attached at the center-of-mass of each quadrotor, the Newton-Euler dynamics of the n-quadrotors and the SmQ-frame can be written as:

$$\begin{aligned}
&m_i \dot{v}_i + S(\omega_i) m_i v_i = m_i g R_i^T e_3 + R_i^T N_i^w - R_i^T R_o \Lambda_i^o \\
&J_i \dot{\omega}_i + S(\omega_i) J_i \omega_i = \tau_i \\
&m_o \dot{v}_o + S(\omega_o) m_o v_o = m_o g R_o^T e_3 - \sum_{i=1}^{n} R_o^T N_i^w + f_e^o \\
&J_o \dot{\omega}_o + S(\omega_o) J_o \omega_o = -\sum_{i=1}^{n} S(x_i^o) R_o^T N_i^w + \tau_e^o
\end{aligned} \tag{3}$$

where $m_i > 0, J_i \in \Re^{3\times3}$ and $m_o > 0, J_o \in \Re^{3\times3}$ are the mass and inertia of the i-th quadrotor and the frame respectively, $g \in \Re$ is the gravity acceleration, $v_i := R_i^T \dot{x}_i^w \in \Re^3$, $v_o := R_o^T \dot{x}_o^w \in \Re^3$ and $\omega_i, \omega_o \in \mathfrak{so}(3)$ are their body translation and angular velocities represented in their body-fixed frames $\{\mathcal{F}_i\}$ and $\{\mathcal{F}_0\}$ with the superscripts omitted for simplicity, $N_i^w \in \Re^3$ is the constraint force to enforce the constraint (1), $\Lambda_i^o = \lambda_i R_o^T R_i e_3$ is the thrust force vector constrained according to (2), $\tau_i \in \Re^3$ is the torque control input of the i-th quadrotor, $S(\omega)$ is the skew-symmetric matrix such that $S(\omega)\nu = \omega \times \nu, \forall \omega, \nu \in \Re^3$, and $f_e^o, \tau_e^o \in \Re^3$ are the external force and torque acting at the center-of-mass of the SmQ-frame.

By eliminating the constraint forces N_i^w in (3) of the constraint (1), we can reduce the dynamics (3) into the lumped

[2]We use the superscript throughout the paper to specify in which frame the entity is expressed if deemed beneficial to eliminate confusion (e.g., x_i^w and x_i^o in (1) denote the same x_i expressed in $\{\mathcal{F}_W\}$ and in $\{\mathcal{F}_0\}$, respectively).

6-DOF dynamics of the SmQ-platform in SE(3) and the $3n$-DOF attitude dynamics of the n-quadrotors. First, the reduced 6-DOF SmQ-frame dynamics can be obtained s.t.,

$$M\dot{\xi} + C\xi + G = U + F_e \tag{4}$$

where $\xi := [v_c; \omega_o] \in \Re^6$ with v_c being the body translation velocity of the center-of-mass of the total system expressed in $\{\mathcal{F}_0\}$ as defined by

$$v_c := R_o^T \frac{d}{dt} \underbrace{\left[\frac{1}{\sum_{i=0}^n m_i} \sum_{i=0}^n m_i x_i^w\right]}_{=:x_c^w} \in \Re^3 \tag{5}$$

and

$$M := \begin{bmatrix} \bar{m}I & 0 \\ 0 & \bar{J} \end{bmatrix},$$
$$\bar{m} := \sum_{i=0}^n m_i,\ \bar{J} := J_o - \sum_{i=1}^n m_i S(x_i^o) S(x_i^o - x_c^o),$$
$$C := \begin{bmatrix} S(\bar{m}\omega_o) & 0 \\ 0 & -S(\bar{J}\omega_o) \end{bmatrix},$$
$$G := \begin{bmatrix} -\bar{m} g R_o^T e_3 \\ 0 \end{bmatrix}, \quad F_e = \begin{bmatrix} f_e^o \\ \tau_e^o \end{bmatrix}$$

are the lumped (symmetric/positive-definite) inertia matrix, the (skew-symmetric) Coriolis matrix, the gravity effect and the external forcing, respectively,

$$U := -B\Lambda \in \Re^6 \tag{6}$$

is the control input to the SmQ-platform, where $\Lambda := [\Lambda_1^o; \Lambda_2^o; ...; \Lambda_n^o] \in \Re^{3n}$ is the collective rotating thrust vectors, and

$$B(d) := \begin{bmatrix} I & I & ... & I \\ S(d_1) & S(d_2) & ... & S(d_n) \end{bmatrix} \in \Re^{6\times 3n} \tag{7}$$

is the mapping matrix, which defines how the thrust actuation of each quadrotor affects the SmQ-platform dynamics depending on its mechanical structure design (i.e., design of d_i), with $d_i := x_i^o - x_c^o \in \Re^3$. On the other hand, the attitude dynamics of each quadrotor is given by:

$$J_i\dot{\omega}_i + S(\omega_i)J_i\omega_i = \tau_i, \tag{8}$$

which constitutes the $3n$-DOF attitude dynamics of the n-quadrotors in $\mathrm{SO}^n(3)$ in addition to the 6-DOF reduced dynamics of the SmQ-platform (4).

Note that, due to our design of connecting the spherical joint at the center-of-mass of the quadrotors, the attitude dynamics of each quadrotor (8) is decoupled from the SmQ-platform dynamics (4). This attitude dynamics of the quadrotor can be typically controlled much faster than the SmQ-platform dynamics. This then means that we can consider $\Lambda_i^o = \lambda_i R_o^T R_i e_3 \in \Re^3$ as the control input for (4) and the n-quadrotors as rotating thrust actuators for the 6-DOF SmQ-platform dynamics (4) with the fast-enough low-level attitude control embedded for each quadrotor (see Sec. VI).

We can also see that the structure of $B(d) \in \Re^{6\times 3n}$ in (4) dictates whether we can generate an arbitrary control action $U \in \Re^6$ by using the thrust inputs Λ_i^o of the n-quadrotors. This structure of $B(d)$ depends on the the number of quadrotors n and the arrangement of the attaching points x_i^o (see Fig. 1). In the next Sec. III, we analyze how this structure design of the SmQ-platform is related to its actuation capacity and also when a given task is guaranteed to be feasible for the SmQ-platform system under the range constraint of the spherical joint (2) and the thrust actuation bound $\bar{\lambda}_i$.

III. Control Generation and Feasibility Analysis

For the control of the 6-DOF SmQ-platform dynamics (4), it is desirable to generate any arbitrary control input $U \in \Re^6$ by recruiting the thrust actuation Λ_i of the n-quadrotors. This, yet, is not in general possible, since the thrust actuation of each quadrotor $\Lambda_i \in \Re^3$ is constrained by the spherical joint rotation range (2) and the thrust generation bound $\bar{\lambda}_i$. This control generation may also be limited depending on the SmQ-platform design, i.e., the structure of the mapping matrix $B(d)$ in (7). At the same time, we would like to minimize any internally-dissipated thrust actuation as much as possible. This problem, that is, how to optimally realize a desired control wrench $U \in \Re^6$ for the SmQ-platform by using n-quadrotors as rotating thrust generators under the constraints can be formulated as the following constrained optimization problem:

$$\Lambda_{\text{op}} = \underset{\Lambda=(\Lambda_i,\Lambda_2,...,\Lambda_n)}{\arg\min} \frac{1}{2}\Lambda^T\Lambda \tag{9}$$

subject to

$$B(d)\Lambda = -U \tag{10}$$
$$\Lambda_i^T[\cos^2\phi_i I_{3\times 3} - p_i p_i^T]\Lambda_i \le 0 \tag{11}$$
$$\Lambda_i^T\Lambda_i - \bar{\lambda}_i^2 \le 0 \tag{12}$$

where (9) is to maximize energy efficiency by eliminating internally-dissipated thrust generations (or to minimize internal forces producing no net platform motion), (10) is to generate the desired control wrench $U \in \Re^6$, (11) is the spherical joint motion range constraint written in a matrix form, and (12) is to reflect the boundedness of the thrust actuation Λ_i. The desired platform control $U \in \Re^6$ will be designed based on Lyapunov design in Sec. IV-A and Sec. V-B, which is then optimally decoded into each rotor thrust Λ_i while respecting the constraints (11)-(12). This means that our (closed-loop) control strategy is hierarchical, consisting of high-level Lyapunov control design and low-level constrained optimization. See Sec. IV (for S3Q system) and Sec. V (for S2Q system).

The constrained optimization (9)-(12) is a second-order cone programming (SOCP), which is a convex optimization problem [27]. Further, feasibility and continuity of the desired control $U \in \Re^6$ for (10) is to be ensured via the task planning as stated in Sec. III-B. With its convexity and the continuity of its constraints and objective function, the solution continuity of this constrained optimization (9)-(12) follows [28]. This constrained optimization (9)-(12) also has similarity with the multi-finger grasping problem under friction-cone constraint [11], which we will exploit in the sequel to solve this (9)-(12) and also to analyze some salient SmQ-platform behaviors. For

the SmQ-platform, this constrained optimization will be real-time solved during the operation given the desired platform control $U \in \Re^6$, for which dimension reduction turns out to be instrumental (see Sec. IV-B and Sec. V-C). Design of U and its real-time optimal allocation to Λ_i for the specific S3Q-platform and S2Q-platform are the topics of Sec. V and Sec. IV. Instead, in this Sec. III, analyzing (10)-(12), we present some conditions on the mechanical structure design for the full-actuation of the SmQ-platform in SE(3) and further propose a framework to design the task (i.e., U) so that its feasibility under the constraints (10)-(12) is guaranteed.

A. Necessary Rank Condition for Full-Actuation in SE(3)

Now, let us focus only on the first condition (10) of the constrained optimization problem. Then, since $U \in \Re^6$ can in general be an arbitrary control command, the existence of the solution, $\Lambda \in \Re^{3n}$, depends on the rank of the matrix $B(d) \in \Re^{6\times 3n}$. As can be seen from (7), $B(d)$ is a function of only mechanical design parameters d_i (i.e., the attaching point of quadrotors on the SmQ-frame). In other words, this d_i affects the structure of B, which in turn decides the existence of solution for (10). This suggests us to choose these mechanical design parameters, d_i, $i = 1, 2, ..., n$, to ensure that:

$$\text{rank}(B) = 6 \tag{13}$$

Note that this rank condition (13) is necessary for the 6-DOF SmQ-platform (4) to be fully-actuated in SE(3). The next Prop. 1 shows that, for the 6-DOF full-actuation of the SmQ-platform, the number of deployed quadrotors should be at least three and the configuration of their attaching points (i.e., $d_i \in \Re^3$) should avoid certain "singular" configurations.

Proposition 1. *Consider the SmQ-platform* (4) *consisting of n-quadrotors connected via spherical joints. Then, the necessary rank condition* (13) *for its full-actuation in SE(3) is granted, if and only if there are at least three quadrotors with their attaching points d_i (expressed in $\{\mathcal{F}_0\}$) not collinear with each other, i.e.,*

$$(d_2 - d_1) \times (d_3 - d_1) \neq 0 \tag{14}$$

Proof. First, we consider the case where there are three quadrotors attached to the tool/frame, whose attaching points d_i are not collinear as stated above. Then, the control wrench generation for the SmQ-platform by these three quadrotors is given by

$$B\Lambda = \begin{bmatrix} I & I & I \\ S(d_1) & S(d_2) & S(d_3) \end{bmatrix} \begin{bmatrix} \Lambda_1 \\ \Lambda_2 \\ \Lambda_3 \end{bmatrix}$$

where we can decompose B s.t.,

$$B = \underbrace{\begin{bmatrix} I & 0 \\ S(d_1) & I \end{bmatrix}}_{:=L} \underbrace{\begin{bmatrix} I & 0 & 0 \\ 0 & S(d_2 - d_1) & S(d_3 - d_1) \end{bmatrix}}_{:=\Sigma} \underbrace{\begin{bmatrix} I & I & I \\ 0 & I & 0 \\ 0 & 0 & I \end{bmatrix}}_{:=D}$$

by using the linearity of the operator $S(\star)$. We can then see that $\text{rank}(B) = \text{rank}(\Sigma)$, since L and D are both full-rank. We now show that $\text{rank}(\Sigma) = 6$ if and only if the non-collinear condition (14) is ensured with the three quadrotors, i.e., for the S3Q-platform. For this, recall that $\text{rank}(S(\nu)) = 2\ \forall \nu \neq 0$. Thus, we have

$$\text{rank}(\Sigma) = 3 + \text{rank}(\begin{bmatrix} S(d_2 - d_1) & S(d_3 - d_1) \end{bmatrix})$$

Suppose that the non-collinear condition (14) is satisfied, yet, $\text{rank}(\Sigma) < 6$. Then, there should exists $y \in \Re^3$ s.t., $y^T[S(d_2 - d_1)\ S(d_3 - d_1)] = 0$. This then implies $y = k_1(d_2 - d_1) = k_2(d_3 - d_1)$ for some $k_1, k_2 \in \Re$, which yet results in $(d_2 - d_1) \times (d_3 - d_1) = 0$, contradicting the non-collinear assumption (14). Note that addition of more quadrotors to the S3Q-platform with the non-collinear condition (14) will still ensure the necessary rank condition (13). Consider also the case that there are only two quadrotors, i.e., the S2Q-platform or all the quadrotors in the system are attached collinear with each other. We can then easily show that $\text{rank}(\Sigma) \leq 5$, thus, the platform is underactuated. This completes the proof. □

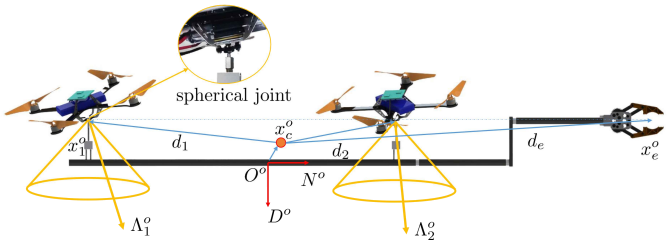

Fig. 3: S2Q-platform with the two quadrotors and the tool, where we assume: 1) d_1, d_2, d_e are within the plane spanned by the N^o and E^o axes of $\{\mathcal{F}_O\}$; 2) $d_2 - d_1$ and $d_e - d_1$ are all parallel to the N^o-axis with (17); and 3) the spherical joint center axes p_i are all along the D^o-axis of $\{\mathcal{F}_O\}$.

The Prop. 1 characterizes "singular" designs of the SmQ-platform, that should be avoided if the full-actuation in SE(3) is necessary. It is however worthwhile to mention that, even if a SmQ-platform is not fully-actuated in SE(3) (i.e., the condition (13) not satisfied), it may be able to provide limited, yet, still useful motion capability. For instance, consider the S2Q-platform system as shown in Fig. 3 with

$$B(d) := \begin{bmatrix} I & I \\ S(d_1) & S(d_2) \end{bmatrix} \in \Re^{6\times 6}$$

We can then verify that:

$$\begin{bmatrix} d_2^T S^T(d_1) & (d_2 - d_1)^T \end{bmatrix} B\Lambda = 0,\ \forall \Lambda \in \Re^6 \tag{15}$$

that is, if $d_1 \neq d_2$, $\text{rank}[B] = 5$ and

$$\text{null}[B^T] \approx \begin{pmatrix} S(d_1)d_2 \\ d_2 - d_1 \end{pmatrix} = \begin{bmatrix} I & S(d_1) \\ 0 & I \end{bmatrix} \begin{pmatrix} 0 \\ d_2 - d_1 \end{pmatrix} \tag{16}$$

This null motion is in fact a pure rotation of the S2Q-platform about the $(d_2 - d_1)$-axis, with $(0; d_2 - d_1)$ and $(S(d_1)d_2; d_2 - d_1)$ in (16) respectively being the body velocity of the (N,E,D)-coordinate frames attached at x_1 and x_c with the same attitude, and the mapping between them an adjoint operator [11]. For the S2Q-system in Fig. 3 with x_1, x_2, x_e all on the same line with

$$(d_e - d_1) \times (d_2 - d_1) = 0 \tag{17}$$

this then implies that the system can only generate 5-DOF actuation with the moment about the N^0-axis (i.e., $x_2^o - x_1^o$) of the tool-tip frame $\{\mathcal{F}_E\}$ not generatable/resistable. Even so, by designing the tool-tip located at $d_e \in \Re^3$ in Fig. 3, we can still fully control the tool-tip translation in $\Re^3$ as well as its pointing direction in S^2. The roll rotation of the tool-tip is not controllable, which, yet, may not be so detrimental for such applications as pushing/pulling task, button operation, assembly of parts symmetric about the N^0-axis, contact probe operation, etc. Of course, if the full-actuation in SE(3) is necessary, we may use a SmQ-platform with $m \geq 3$ and designed with the non-collinear condition (14) ensured.

B. Control Feasibility

Now, suppose that we have a SmQ-platform satisfying Prop. 1. This then ensures that there exists thrust vectors $\Lambda_i \in \Re^3$, $i = 1, 2, ..., n$ for (10) to produce any desired platform control $U \in \Re^6$. This, however, is true only if Λ_i is not constrained, and what is unclear is whether these solution thrust vectors Λ_i would also respect the constraints (11) and (12). We say the control wrench $U \in \Re^6$ is feasible if there exists a solution $\Lambda = (\Lambda_1, \Lambda_2, ..., \Lambda_n) \in \Re^{3n}$, which also complies with the constraints (11) and (12). In this Sec. III-B, we analyze this control feasibility of the SmQ-platforms and also show how to design a task for them while guaranteeing this control feasibility.

For this, we would first like to recognize that this control feasibility of the SmQ-platform is analogous to the force-closure of the multi-fingered grasping under the friction cone constraint. More precisely, notice from Fig. 2 that each thrust vector Λ_i of the SmQ-platform is confined within the cone defined by the limited motion range of their spherical joint. The control feasibility problem then boils down to the question whether a given desired control wrench $U \in \Re^6$ can be generated by the thrust vectors Λ_i each residing in their respective cone. This is exactly the same question of the force closure [11], [29], i.e., whether it is possible to resist an external wrench by using the contact force of multiple fingers, with its normal and shear forces constrained to adhere Coulomb friction model (i.e., cone with the angle specified by the friction coefficient μ). The following Prop. 2 is due to this analogy between the control feasibility and the force closure.

Proposition 2. *For the SmQ-platforms satisfying Prop. 1, we can generate any control wrench $U \in \Re^6$ in* (10) *for the platform using the thrust vectors $\Lambda_i \in \Re^3$, $i = 1, 2, ..., n$, while respecting the constraints* (11)-(12)*, if and only if the desired wrench U_d is in force closure with $\Lambda_i \in \Re^3$ being the contact forces residing inside their friction cone defined by the constraints* (11)-(12)*.*

To ensure the control feasibility of the SmQ-platform, we may take one of the following two approaches. The first is to real-time solve the desired control wrench $U \in \Re^6$ and the collective thrust vectors Λ_i, $i = 1, 2, ...n$ simultaneously to drive the SmQ-platform (4) according to a certain task objective while also taking into account all the constraints (10)-(12) in a manner similar to the technique of MPC (model predictive control). This approach, yet, typically results in a computationally-complex algorithm, the real-time running of which is often challenging in practice. Instead, in this paper, we adopt the other "task-design" approach, where we first construct the (quasi-static) feasible control set $\mathcal{U} \in$ se(3) (expressed in the body-frame $\{\mathcal{F}_0\}$) under the constraints (11)-(12):

$$\mathcal{U} := \{U = B\Lambda \mid p_i^T \Lambda_i \geq \|\Lambda_i\| \cos\phi_i, \|\Lambda_i\| \leq \bar{\lambda}_i\}$$

and design the task in such a way that its required control U is always within this $\mathcal{U}$, thereby, guaranteeing the control feasibility. This "task-design" approach also allows for an hierarchical control architecture, where $U \in \Re^6$ for (4) (via (10)) is computed using, e.g., Lyapunov-based control design for the task, which is designed *a prior* for control feasibility, while the constrained optimization (9)-(12) is real-time solved given the control U with the solution existence always guaranteed. See Sec. IV-B and Sec. V-C.

The control feasible sets $\mathcal{U}$ of the S2Q-platform (Fig. 3) and S3Q-platform (Fig. 1) are shown in Fig. 4, where the feasible control force set $\mathcal{U}_f$ and the feasible control moment set $\mathcal{U}_\tau$ are separately presented. For this, we use the parameters of the S2Q-platform and S3Q-platform prototypes in Sec. VI. The cross dots represent the gravity wrench $G = [g_f; g_\tau] \in \Re^6$ in (4) expressed in $\{\mathcal{F}_0\}$ at the hovering posture (i.e., $R_o = I$), which the control wrench U_d should always compensate for to maintain flying. Note from Fig. 4a that, due to its under-actuation (with the condition (13) not granted - see Prop. 1), $\mathcal{U}_\tau$ of the S2Q-platform is given by surface instead of volume. For a given task, we can then examine its feasibility by drawing its required control U_d and seeing if it is within this set $\mathcal{U}$ or not before performing the task.

Here, note that the feasible set $\mathcal{U}$ is convex with the hovering wrench G strictly within its interior. This then means that, if the desired motion and contact wrench are small enough and also so are the uncertainty and initial error, there always exists control input U within $\mathcal{U}$ in the neighborhood of G (i.e., solution existence guaranteed). To better show this, we draw the control inputs of two time-scaled trajectories in Fig. 4 for the S2Q and S3Q systems, respectively. The slower (i.e., smaller/red orbits in Fig. 4) is in fact that used during the experiments in Sec. VI-B and Sec. VI-C and we can see that it is feasible satisfying the constraints (11)-(12); whereas the faster (i.e., larger/blue orbits in Fig. 4) is not feasible since some of its trajectory are outside of $\mathcal{U}$. If we further slow down the trajectory, the control trajectory will further shrink and eventually converge to the point of G. This task-design approach to ensure the control feasibility is rather conservative. How to more aggressively transverse the feasible set $\mathcal{U}$ by adopting some dynamics-based planning for the SmQ system is a topic for future work, for which standard motion planning techniques are rather limited, since the control force/moment input sets, $\mathcal{U}_f$ and $\mathcal{U}_\tau$, of the SmQ systems are not independent from each other as typically assumed in the motion planning literatures.

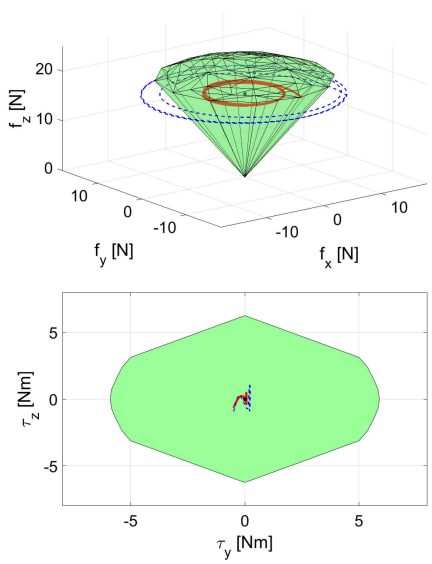

(a) Feasible set $\mathcal{U}$ of the S2Q-platform in Fig. 3.

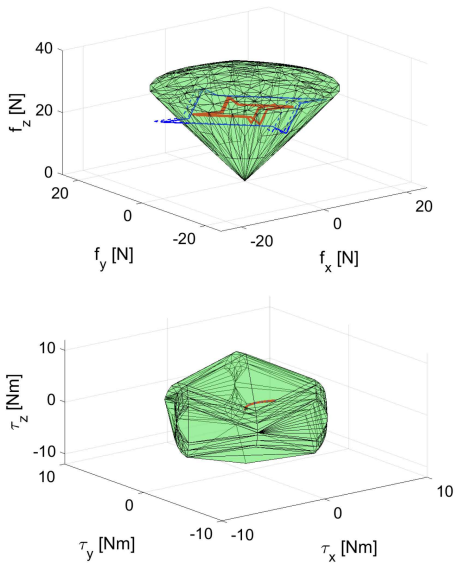

(b) Feasible set $\mathcal{U}$ of the S3Q-platform in Fig. 1.

Fig. 4: (Top) Feasible force sets $\mathcal{U}_f$ and (bottom) feasible moment sets $\mathcal{U}_\tau$ of the S2Q-platform and S3Q-platform systems. The blue dash lines represent the required control wrenches for the infeasible (aggressive) motion tracking tasks. The red solid lines are the control wrenches implemented in Sec. VI with the performance presented in Fig. 9a and Fig. 8a, respectively. The cross dots are the gravity wrench G at the hovering posture, which is also the required control wrench U_d for stabilization control in Sec. VI.

IV. Control of S3Q-Platform System

In this Sec. IV, we consider the tracking control problem of the S3Q-platform system of Fig. 1. With the rank condition of Prop. 1 and the control feasibility of Prop. 2 satisfied, the S3Q-platform system becomes fully-actuated with the solution of the control allocation (9)-(12) always guaranteed to exist, thereby, rendering the tracking problem in $\Re^3 \times$SO(3) rather straightforward. This then means that we can freely control the position and orientation of a mechanical tool (e.g., drill, driver, etc.) rigidly attached to the S3Q-platform for performing aerial operation tasks. Similar tracking control is also addressed for the S2Q-platform system in Sec. V, where its under-actuation (see Sec. III-A) substantially complicates the control design and analysis.

Let us denote the tool-tip position by $x_e \in \Re^3$ and the tool attitude by $R_o \in$ SO(3). We then have the following relation between the tool pose $(x_e^w, R_o) \in$SE(3) and the platform pose (x_c^w, R_o):

$$x_e^w = x_c^w + R_o d_e, \qquad \dot{x}_e^w = R_o v_c + R_o S(\omega_o) d_e \tag{18}$$

where $x_e^w, x_c^w \in \Re^3$ are x_e, x_c expressed in $\{\mathcal{F}_W\}$, $d_e \in \Re^3$ is the vector from the system center-of-mass x_c to x_e expressed in $\{\mathcal{F}_0\}$ (i.e., $d_e = x_e^o - x_c^o$), and v_c is defined in (5). The control objective is then to design $U \in \Re^6$ in (4) s.t.

$$(x_e^w(t), R_o(t)) \to (x_d^w(t), R_d(t))$$

while satisfying the constraints (10)-(12), where $(x_d^w(t), R_d(t)) \in$ SE(3) is the timed-trajectory of the desired tool pose (specified by the coordinate frame $\{\mathcal{F}_D\}$ and expressed in $\{\mathcal{F}_W\}$) and is assumed to be planned off-line to ensure its feasibility as explained in Sec. III-B.

A. Lyapunov-Based Control Design

To design $U \in \Re^6$ in (4) to achieve the tracking as stated above, we define a smooth non-negative potential function on SE(3) s.t.,

$$\Phi := \frac{1}{2} k_x e_x^T e_x + k_r \Psi_R$$

where $k_x, k_r \in \Re$ are positive gains, and

$$e_x = x_e^w - x_d^w, \quad \Psi_R = \frac{1}{2} \operatorname{tr}(\eta - \eta R_d^T R_o)$$

with $\eta = \operatorname{diag}[\eta_1, \eta_2, \eta_3] \in \Re^{3\times 3}$ and η_1, η_2, η_3 being distinct positive constants. This potential Φ has following properties: 1) $\Phi \geq 0$ with the equality hold iff $(x_e^w, R_o) = (x_d^w, R_d)$; 2) its derivative is given by

$$\dot{\Phi} = \nabla\Phi \cdot (\xi - \xi_d)$$

where $\nabla\Phi \in \Re^{1\times 6}$ is the one-form of Φ defined s.t.,

$$\nabla\Phi^T = \begin{bmatrix} I & 0 \\ -S(d_e) & I \end{bmatrix} \begin{bmatrix} k_x R_o^T e_x \\ k_r (\eta R_d^T R_o - R_o^T R_d \eta)^\vee \end{bmatrix} \in \Re^6$$

$$\xi_d := \begin{bmatrix} S(d_e) R_o^T R_d \omega_d + R_o^T R_d v_d, \\ R_o^T R_d \omega_d \end{bmatrix} \in \Re^6$$

where $v_d, \omega_d \in \Re^3$ are the desired velocities expressed in $\{\mathcal{F}_D\}$ as defined by:

$$\dot{x}_d^w = R_d v_d, \qquad w_d = (R_d^T \dot{R}_d)^\vee \tag{19}$$

and $\vee : \Re^{3\times 3} \to \mathfrak{so}(3)$ is the inverse operator of $S(\star)$.

We then design the control $U \in \Re^6$ in (4) s.t.

$$U = M\dot{\xi}_d + C\xi_d - k_v e_\xi - \nabla\Phi^T + G - F_e \tag{20}$$

where $e_\xi := \xi - \xi_d$ with the damping gain $k_v > 0$. The closed-loop dynamics (4) of the S3Q system with (20) is then given by

$$M\dot{e}_\xi + Ce_\xi + k_v e_\xi + \nabla\Phi^T = 0 \tag{21}$$

using which we can show that the SE(3) pose of the S3Q system will converge to the desired one almost everywhere as formalized in the following Th. 1. Here, the convergence is almost everywhere, i.e., except some unstable equilibriums, which in fact stems from the inherent topology of SO(3), yet, can rather easily be avoided in practice by running the operations close enough to the desired pose trajectory - see [30], [31].

Theorem 1. *Consider the dynamics of S3Q-platform* (4) *with the control* U *as designed in* (20)*, which is assumed to satisfy the control feasibility condition of Prop. 2. Then,* $\xi \to \xi_d$ *and*

$$(x_e^w, R_o) \to (x_d^w, R_d)$$

asymptotically almost everywhere except unstable equilibriums $\mathcal{E} := \{(x_e^w, R_o) \mid x_e^w = x_d^w, R_d^T R_o \in \{\mathrm{diag}[-1,-1,1], \mathrm{diag}[-1,1,-1], \mathrm{diag}[1,-1,-1]\}\}$.

Proof. Define the Lyapunov function as follows:

$$V := \Phi + \frac{1}{2} e_\xi^T M e_\xi$$

which is a positive-definite function on SE(3)×se(3) with $V = 0$ iff $(x_e^w, R_o, \xi) = (x_d^w, R_d, \xi_d)$. The derivative of V along the closed-loop dynamics (21) is then given by

$$\dot{V} = \nabla\Phi e_\xi + e_\xi^T(-Ce_\xi - k_v e_\xi - \nabla\Phi^T) = -k_v e_\xi^T e_\xi \leq 0$$

where C is skew-symmetric from the passivity of the system (4), i.e., $\dot{M} - 2C$ is symmetric with $\dot{M} = 0$ (see after (5) for the definition of C). Integrating this, we can further obtain:

$$V(T) - V(0) = -k_v \int_o^T \|e_\xi\|^2 dt$$

$\forall T \geq 0$. This then implies $e_\xi \in \mathcal{L}_\infty \cap \mathcal{L}_2$. We also have $\Phi(t) \leq V(t) \leq V(0), \forall t \geq 0$, thus $\nabla\Phi^T \in \mathcal{L}_\infty$ as well. From (21) with the assumption that v_d^o, ω_d^o and their derivatives be bounded, we then have $\dot{e}_\xi \in \mathcal{L}_\infty$. Using Barbalat's lemma [32], we can then conclude that $e_\xi \to 0$. Differentiating (21), we can also show that $\ddot{e}_\xi \in \mathcal{L}_\infty$ and, applying Barbalat's lemma again, we have $\dot{e}_\xi \to 0$. Applying $(e_\xi, \dot{e}_\xi) \to 0$ to (21), we have $\nabla\Phi^T = 0$. This then means that $e_x = 0$ and, further,

$$(\eta R_d^T R_o - R_o^T R_d \eta)^\vee = 0$$

which, following [30], [31], suggests the almost global asymptotic stability of $R_o \to R_d$ as stated above. This completes the proof. □

B. Optimal Control Allocation

To decode the designed control U in (20) into the thrust vector of each quadrotor, we solve the constrained optimization (9)-(12), which is a convex SOCP with affine equality constraint (10), convex inequality constraints (11)-(12) and convex object function (9). As explained in Sec. III-B, this problem is in fact similar to the robot grasping problem under the friction-cone constraint. To solve this optimization problem (9)-(12) in real-time, here, we employ the barrier method [27] to convert the problem to an unconstrained optimization problem. For this, we exploit the peculiar structure of (9)-(12) to reduce the size of the problem, thereby, significantly speeding up the computation time.

More specifically, we write the general solution of (10) s.t.,

$$\Lambda := -B^T[BB^T]^{-1}U + Z\gamma$$

where $B^T[BB^T]^{-1} \in \Re^{9\times 6}$ is the Moore-Penrose pseudo-inverse of $B(d)$ in (10), $Z \approx \mathrm{null}[B(d)] \in \Re^{9\times 3}$ (i.e., identifies the null-space of $B(d)$), and $\gamma \in \Re^3$ is associated with the internal force term. Utilizing the structure of $B(d)$ in (7), we can write this general solution of (10) for each thrust vector Λ_i s.t.,

$$\bar{\Lambda}_i(\gamma) = \Lambda_i^\dagger + Z_i\gamma \tag{22}$$

where

$$\Lambda_i^\dagger := -[I \ -S(d_i)](BB^T)^{-1}U \in \Re^3$$

and $Z =: [Z_1; Z_2; Z_3]$ with $Z_i \in \Re^{3\times 3}$. Here, note that the only unknown is $\gamma \in \Re^3$. We can then reduce the size of the original optimization problem (9)-(12) by writing that with this $\gamma \in \Re^3$ as the new optimization variable s.t.,

$$\gamma_{\mathrm{op}} = \underset{\gamma\in\Re^3}{\arg\min} \ \frac{1}{2}\sum_{i=1}^{3} \bar{\Lambda}_i^T(\gamma)\bar{\Lambda}_i(\gamma) \tag{23}$$

subject to

$$\mathcal{C}_{1,i} := \bar{\Lambda}_i^T(\gamma)(\cos^2\phi_i I - p_i p_i^T)\bar{\Lambda}_i(\gamma) \leq 0 \tag{24}$$

$$\mathcal{C}_{2,i} := \bar{\Lambda}_i^T(\gamma)\bar{\Lambda}_i(\gamma) - \bar{\lambda}_i^2 \leq 0 \tag{25}$$

Following the procedure of the *barrier method* [27], we then convert (23)-(25) into the following unconstrained optimization:

$$\gamma_{\mathrm{op}} = \underset{\gamma\in\Re^3}{\arg\min} \ \sum_{i=1}^{3} [s\Pi_i(\gamma) + \Xi_i(\gamma)] \tag{26}$$

where $\Pi_i(\gamma) := \frac{1}{2}\bar{\Lambda}_i^T(\gamma)\bar{\Lambda}_i(\gamma)$ is from (23) and $\Xi_i(\gamma) := -\log(-\mathcal{C}_{1,i}(\gamma)) - \log(-\mathcal{C}_{1,i}(\gamma))$ is a logarithmic barrier function to enforce the constraints (24)-(25), and $s \in \Re$ balances between the cost minimization and the constraint enforcement. We then apply the standard way to solve this barrier method, i.e., solve a sequence of unconstrained problem (26) by using the Newton iteration for increasing value of s until $s > \frac{2n}{\epsilon}$, where n is the number of quadrotors and $\epsilon > 0$ is the desired tolerance. The solution of (26) is known to be the $\frac{2n}{s}$-suboptimal solution of (23)-(25) with $n = 3$ for the S3Q system [27].

We implement and run this optimization-solving algorithm in real-time for our S3Q-platform system as experimented in Sec. VI. From this size reduction, we can obtain the closed-form solution of the inverse of a certain Hessian matrix H, which is important for the Newton iteration and, in this case, it is positive definite and also of only the dimension of 3×3. This greatly helps to speed up our solving the optimization problem (26). It is also well-known that the convergence of Newton iteration is quadratic and guaranteed within the

bounded number of iterations [27]. For our experiment in Sec. VI, we observe that this Newton iteration only requires at most 20 iterations for each s, and, including the s-scaling procedure and computing feasible starting point [27], the total control allocation algorithm can run with around 500Hz (on a PC with Intel i7 3.2 GHz CPU), which is proved to be adequate for the experiment. See Sec. VI.

V. Control of S2Q-Platform System

In this Sec. V, we consider motion control problem of S2Q-platform system as shown in Fig. 3 with (17). As elucidated in Sec. III-A, this S2Q-platform system is (frame) under-actuated with only 5-DOF actuation possible for its frame motion in SE(3) (see (15)). Even so, we can still achieve some limited, yet, useful behavior by using this S2Q-platform system, e.g., controlling the tip position and the pointing direction of a tool rigidly attached to the S2Q-system as shown in Fig. 3. The tracking control of this tool-tip position and direction in $\Re^3\times \mathrm{S}^2$ of the S2Q-platform in Fig. 3 is the topic of this Sec. V. As compared to the case of the S3Q-platform tracking control in SE(3) of Sec. IV, this tracking control of the S2Q-platform in $\Re^3\times \mathrm{S}^2$ is more complicated due to the under-actuation.

For this, similar to (18), we denote the tool-tip position by x_e. We also use the line connecting the center-of-mass positions of two quadrotors as the pointing direction of the tool - see Fig. 3. We denote this line by $r_e \in \mathrm{S}^2$, which can be expressed in $\{\mathcal{F}_W\}$ and in $\{\mathcal{F}_0\}$ by

$$r_e^w = R_o r_e^o, \quad r_e^o = (d_2 - d_1)/\|d_2 - d_1\| \tag{27}$$

where r_e^o is a unit constant vector. The tracking control objective for the under-actuated S2Q-platform can then be written by

$$(x_e^w(t), r_e^w(t)) \to (x_d^w(t), r_d^w(t)) \tag{28}$$

where $(x_d^w(t), r_d^w(t)) \in \Re^3\times \mathrm{S}^2$ are the timed-trajectory of the desired tool-tip position and its pointing direction expressed in $\{\mathcal{F}_W\}$. Here, we construct $r_d^w(t) \in \mathrm{S}^2$ by defining $R_d(t) \in$ SO(3) s.t.,

$$r_d^w(t) := R_d(t) r_e^o \tag{29}$$

Note that, given r_d^w and r_e^o, this $R_d(t)$ is not unique. The time-derivative of these r_e^w and r_d^w are then computed by:

$$\dot{r}_e^w = R_o S(\omega_o) r_e^o, \quad \dot{r}_d^w = R_d S(w_d) r_e^o \tag{30}$$

where $w_d \in \mathfrak{so}(3)$ is the angular rate of the coordinate frame $\{\mathcal{F}_D\}$ specified by $R_d \in$ SO(3) and expressed in $\{\mathcal{F}_D\}$ as defined in (19). Recall that $\omega_o \in \mathfrak{so}(3)$ is also the body angular velocity of $\{\mathcal{F}_0\}$.

Our goal here is then to design $U \in \Re^6$ in (4) to achieve this tracking objective in $\Re^3\times \mathrm{S}^2$ under the under-actuation limitation (15). The physical constraints (10)-(12) are assumed to be satisfied by designing $(x_d^w(t), r_d^w(t))$ in such a way to enforce control feasibility of Prop. 2. Due to the under-actuation, the S2Q-platform dynamics can split into: 1) fully-actuated 5-DOF dynamics, which will be controlled to attain the tracking objective of (28); and 2) un-actuated 1-DOF dynamics, which constitutes internal dynamics (with $(x_e^w(t), r_e^w(t))$ as 5-DOF output) and whose stability must be established for the tracking control to have any meaning. To facilitate the analysis of these fully-actuated and un-actuated dynamics of the S2Q-platform, here, we utilize passive decomposition [33] as detailed below.

A. Passive Decomposition of S2Q-Platform Dynamics

Recall from (7) that, for the S2Q-platform in Fig. 3, we have:

$$B(d) := \begin{bmatrix} I & I \\ S(d_1) & S(d_2) \end{bmatrix} \in \Re^{6\times 6}$$

with $\mathrm{rank}[B] = 5$ as shown in (15). Following [33], at each configuration $q = (x_c^w, R_o)$ of the S2Q-platform, we can then decompose the tangent (or velocity) space $T_q\mathcal{M} \approx \Re^6$ and the cotangent (or wrench) space $T_q^*\mathcal{M} \approx \Re^6$ s.t.,

$$T_q\mathcal{M} = \Delta_a \oplus \Delta_u, \quad T_q^*\mathcal{M} = \Omega_a \oplus \Omega_u$$

or, in coordinates,

$$\begin{bmatrix} v_c \\ \omega_o \end{bmatrix} = \underbrace{\begin{bmatrix} \Delta_a & \Delta_u \end{bmatrix}}_{=:\Delta\in\Re^{6\times 6}} \begin{bmatrix} \nu_a \\ \nu_u \end{bmatrix}, \quad U = \underbrace{\begin{bmatrix} \Omega_a^T \\ \Omega_u^T \end{bmatrix}}_{=:\Omega^T\in\Re^{6\times 6}} \begin{bmatrix} u_a \\ u_u \end{bmatrix} \tag{31}$$

where: 1) $\Omega_a^T \approx \mathrm{span}[B] \in \Re^{6\times 5}$ denotes the fully-actuated direction; 2) $\Delta_u \approx \mathrm{null}[B^T] \in \Re^{6\times 1}$ the velocity space of the un-actuated dynamics; 3) $\Delta_a = M^{-1}\Omega_a^T(\Omega_a M^{-1}\Omega_a^T)^{-1} \in \Re^{6\times 5}$ the orthogonal complement of Δ_u w.r.t. the M-metric (i.e., $\Delta_a^T M \Delta_u = 0$); and 4) $\Omega_u^T = M\Delta_u(\Delta_u^T M \Delta_u)^{-1} \in \Re^{6\times 1}$ the control space of the un-actuated dynamics with the M-orthogonality. Here, $\nu_a, u_a \in \Re^5$ and $\nu_u, u_u \in \Re$ are respectively the velocity components and transformed control of the S2Q system in the fully-actuated and un-actuated spaces, respectively, with $u_u = 0$ from $U \in \mathrm{span}[B]$. Note also that the following properties hold for (31): 1) $\Delta_a^T M \Delta_u = 0_{5\times 1}$ (orthogonal w.r.t the M-metric); 2) $\Omega\Delta = I_{6\times 6}$; and 3) $\Delta_a^T U = u_a$ and $\Delta_u^T U = 0$.

The coordinate expression of this decomposition is not unique, and, for that, here, following (16), we choose

$$\Delta_u = \begin{pmatrix} S(d_1)d_2 \\ d_2 - d_1 \end{pmatrix} \approx \mathrm{null}[B^T] \tag{32}$$

which, as explained after (16), represents pure rotation motion of the S2Q-platform of Fig. 3 along the tool-tip axis. Then, differentiating (31) with the above Δ_u and substituting them into (4), we obtain:

$$M_a\dot{\nu}_a + C_a\nu_a + C_{au}\nu_u + g_a = u_a + f_a \tag{33}$$

$$M_u\dot{\nu}_u + C_u\nu_u + C_{ua}\nu_a + g_u = u_u + f_u \tag{34}$$

where $M_a := \Delta_a^T M \Delta_a$, $M_u := \Delta_u^T M \Delta_u$,

$$\begin{bmatrix} C_a & C_{au} \\ C_{ua} & C_u \end{bmatrix} := \begin{bmatrix} \Delta_a^T C \Delta_a & \Delta_a^T C \Delta_u \\ \Delta_u^T C \Delta_a & \Delta_u^T C \Delta_u \end{bmatrix}$$

with $C_u = 0$, and (g_a, g_u) and (f_a, f_u) are the transformed gravity G and external wrench F_e in (4) computed similarly to (u_a, u_u) in (31) with $u_u = 0$ (i.e., ν_u-dynamics (16) is un-actuated).

Note that the passive decomposition decomposes the S2Q-platform dynamics (4) into the fully-actuated ν_a-dynamics on

Δ_a with $u_a \in \Re^5$ and the un-actuated ν_u-dynamics on Δ_u with $u_u = 0$. This is done while preserving the Lagrangian structure and passivity of the original dynamics (4), i.e., constant symmetric and positive-definite $M_a \in \Re^{5\times5}$ with skew-symmetric C_a; constant $M_u > 0$ with $C_u = 0$; and $C_{au} + C_{ua}^T = 0$. For more details on passive decomposition, refer to [33] and references therein. These decomposed dynamics (33)-(34) then serve the basis for our control design and internal stability analysis as below.

B. Lyapunov-Based Control Design and Internal Stability

Here, we design the control $U \in \Re^6$ in (4) or, equivalently, $u_a \in \Re^5$ in (33), for the S2Q-platform as shown in Fig. 3 with (17) to achieve the trajectory tracking in $\Re^3\times\mathrm{S}^2$ as stated in (28). First, similar to the case of S3Q-platform control in Sec. IV-A, we define a potential function on $\Re^3\times\mathrm{S}^2$ s.t.,

$$\Phi = \frac{1}{2}k_x e_x^T e_x + k_r\left[1 - (r_d^w)^T r_e^w\right]$$

where $e_x := x_e^w - x_d^w \in \Re^3$ expressed in $\{\mathcal{F}_W\}$, $r_e^w, r_d^w \in \mathrm{S}^2$ are the real and desired pointing direction of the tool as defined in (27) and (29), and $k_x, k_r > 0$ are the gains. Then, we can see that $\Phi \geq 0$ with the equality hold iff $(x_e^w, r_e^w) = (x_d^w, r_d^w)$.

We can then compute the time-derivative of Φ s.t.,

$$\begin{aligned}\dot\Phi &= k_x e_x^T(\dot x_e^w - \dot x_d^w) - k_r(r_e^o)^T\frac{d}{dt}(R_d^T R_o)r_e^o\\ &= k_x e_x^T\left[R_o(v_c - S(d_e)\omega_o) - \dot x_d^w\right] - k_r(r_e^o)^T R_d^T R_o S(e_\omega)r_e^o\\ &= k_x e_x^T R_o\left[v_c - S(d_e)e_\omega - S(d_e)R_o^T R_d\omega_d - R_o^T R_d v_d\right]\\ &\quad + k_r(r_e^o)^T R_d^T R_o S(r_e^o)e_\omega\end{aligned}$$

where we use (18), (19), $\frac{d}{dt}(R_d^T R_o) = R_d^T R_o S(\omega_o - R_o^T R_d\omega_d)$ and $e_\omega := \omega_o - R_o^T R_d\omega_d$, which is the angular rate error expressed in $\{\mathcal{F}_0\}$. Rearranging this, we can further write:

$$\dot\Phi = \begin{pmatrix}k_x R_o^T e_x\\ k_r R_o^T r_d^w\end{pmatrix}^T \underbrace{\begin{bmatrix}I & -S(d_e)\\ 0 & -S(r_e^o)\end{bmatrix}}_{=:\bar S\in\Re^{6\times6}}(\xi - \xi_d) \tag{35}$$

where $\xi = [v_c; \omega_o]$ and

$$\xi_d := \begin{pmatrix}S(d_e)R_o^T R_d\omega_d + R_o^T R_d v_d\\ R_o^T R_d\omega_d\end{pmatrix} \in \Re^6$$

i.e., the desired translation and rotation velocities of the total system center-of-mass expressed in $\{\mathcal{F}_O\}$. This derivative of the potential Φ depends only on the evolution of the S2Q-platform dynamics in Δ_a (33), as can be seen by:

$$\bar S\cdot\Delta_u = \begin{pmatrix}S(d_1)d_2 - S(d_e)(d_2 - d_1)\\ -S(r_e^o)(d_2 - d_1)\end{pmatrix} = 0$$

where we use $d_e := k(d_2 - d_1) + d_1$ from (17) for some constant $k \in \Re$.

Define $\nu_{a_d} \in \Re^5$ and $\nu_{u_d} \in \Re$ s.t.,

$$\xi_d =: \begin{bmatrix}\Delta_a & \Delta_u\end{bmatrix}\begin{pmatrix}\nu_{a_d}\\ \nu_{u_d}\end{pmatrix}$$

with which we can write

$$\dot\Phi = \nabla\Phi\cdot(\nu_a - \nu_{a_d}) \tag{36}$$

where

$$\nabla\Phi := \begin{pmatrix}k_x R_o^T e_x\\ k_r R_o^T r_d^w\end{pmatrix}^T\cdot\bar S\cdot\Delta_a \in \Re^{1\times5}$$

We then design the control $u_a \in \Re^5$ in (33) s.t.,

$$\begin{aligned}u_a = {}& C_{au}\nu_u + g_a - f_a\\ &+ M_a\dot\nu_{a_d} + C_a\nu_{a_d} - k_v(\nu_a - \nu_{a_d}) - \nabla\Phi^T\end{aligned} \tag{37}$$

with which the closed-loop ν_a-dynamics (33) becomes:

$$M_a\dot e_a + C_a e_a + k_\nu e_a + \nabla\Phi^T = 0 \tag{38}$$

with $e_a := \nu_a - \nu_{a_d}$ and $k_v > 0$.

Theorem 2. *Consider the dynamics* (4) *of the S2Q-platform system of Fig. 3 with the geometric condition* (17) *and the tracking control* (37)*, which is assumed to satisfy the control feasibility of Prop. 2. Define*

$$V := \Phi + \frac{1}{2}e_a^T M_a e_a \tag{39}$$

and suppose that $V(0) < 2k_r$. Then,

$$\nu_a \to \nu_{a_d}, \quad (x_e^w(t), r_e^w(t)) \to (x_d^w(t), r_d^w(t))$$

Proof. Here, we use V in (39) as a Lyapunov function, which is positive-definite with $V = 0$ iff $(x_e^w, r_e^w, \nu_a) = (x_d^w, r_d^w, \nu_{a_d})$. Differentiating V along (38), we obtain:

$$\dot V = \nabla\Phi\cdot e_a + e_a^T[-C_a e_a - k_v e_a - \nabla\Phi^T] = -k_v e_a^T e_a \leq 0$$

where C_a is skew-symmetric from the (preserved) passivity through the passive decomposition (see Sec. V-A). Integrating this, we can then attain

$$V(T) - V(0) = -k_v\int_o^T \|e_a\|^2 dt \leq 0 \tag{40}$$

$\forall T \geq 0$. This implies that $e_a \in \mathcal{L}_\infty \cap \mathcal{L}_2$. Also, since $\Phi(t) \leq V(t) \leq V(0), \forall t \geq 0$, $\nabla\Phi \in \mathcal{L}_\infty$. From (38) with v_d, ω_d and their derivatives being bounded, this then means that $\dot e_a \in \mathcal{L}_\infty$, implying $e_a \to 0$ due to Barbalat's lemma [32]. Differentiating (38), we also can show that $\ddot e_a \in \mathcal{L}_\infty$, implying $\dot e_a \to 0$ again due to Barbalat's lemma. Applying $(e_a, \dot e_a) \to 0$ to (38), we then have $\nabla\Phi^T \to 0$. Since $\Delta_a \in \Re^{5\times5}$ is non-singular, $\nabla\Phi^T \to 0$ then means that:

$$\bar S^T\begin{pmatrix}k_x R_o^T e_x\\ k_r R_o^T r_d^w\end{pmatrix} = \begin{bmatrix}I & 0\\ S(d_e) & S(r_e^o)\end{bmatrix}\begin{pmatrix}k_x R_o^T e_x\\ k_r R_o^T r_d^w\end{pmatrix} \to 0$$

where we have $e_x \to 0$ from the first row, whereas, from the second row, $S(r_e^o)R_o^T r_d^w = R_o^T S(r_e^w)r_d^w \to 0$, implying that $r_e^w \to r_d^w$ or $r_e^w \to -r_d^w$. Here, $r_e^w \to -r_d^w$ is impossible, since, from (40) with $V(0) < 2k_r$ as assumed above, we have: $\forall t \geq 0$,

$$k_r[1 - (r_d^w(t))^T r_e^w(t)] \leq V(t) \leq V(0) < 2k_r$$

where $k_r[1 - (r_d^w(t))^T r_e^w(t)]$ attains its maximum $2k_r$ only when $r_e^w \to -r_d^w$, implying that only $r_e^w \to r_d^w$ is possible. □

The condition of $V(0) < 2k_r$ of Th. 2 is to ensure that the initial error $e_a(0), e_x(0)$ is small enough with $r_e^w(0)$ far enough from $-r_d^w(0)$ so that the attitude of the S2Q system

always converges to the desired equilibrium (i.e., $r_e^w \to r_d^w$). This condition can be easily granted by initiating the tracking operation from, e.g., the steady-state hovering while designing x_d to start close enough from $x_e(0)$. Even though this Th. 2 proves that the tracking objective (28) in $\Re^3 \times \mathrm{S}^2$ is attained with the control (37), it only provides a partial verdict for its practical applicability, as the un-actuated dynamics (34), which in fact constitutes the internal dynamics with the 5-DOF output (x_e, r_e), may become unstable under the control (37).

This internal dynamics is given by the un-actuated ν_u-dynamics (34), which we rewrite here in a more compact form:

$$M_u \dot{\nu}_u + C_{ua}\nu_a + g_u = f_u \tag{41}$$

where

$$g_u = \Delta_u^T G = -\left[\bar{m} g R_o^T e_3\right]^T S(d_1) d_2$$

from (31) with $\bar{m} := \sum_{i=0}^{2} m_i$, which is the moment generated by the gravity about the N^E-axis of the tool-tip frame $\{\mathcal{F}_E\}$. Further, as captured by (16) and explained there, the motion of this ν_u-dynamics, i.e., $\Delta_u \nu_u$ is the pure rotation motion about the same N^E-axis with its magnitude given by $||d_2 - d_1|| \cdot ||\nu_u||$.

To facilitate the stability analysis of this internal dynamics (41), we parametrize the rotation matrix R_o by the yaw, pitch, roll angles $[\phi; \theta; \psi] \in \Re^3$ s.t.,

$$R_o = \begin{bmatrix} \mathrm{c}\,\phi\,\mathrm{c}\,\theta & -\mathrm{s}\,\phi\,\mathrm{c}\,\psi + \mathrm{c}\,\phi\,\mathrm{s}\,\theta\,\mathrm{s}\,\psi & \mathrm{s}\,\phi\,\mathrm{s}\,\psi + \mathrm{c}\,\phi\,\mathrm{s}\,\theta\,\mathrm{c}\,\psi \\ \mathrm{s}\,\phi\,\mathrm{c}\,\theta & \mathrm{c}\,\phi\,\mathrm{c}\,\psi + \mathrm{s}\,\phi\,\mathrm{s}\,\theta\,\mathrm{s}\,\psi & -\mathrm{c}\,\phi\,\mathrm{s}\,\psi + \mathrm{s}\,\phi\,\mathrm{s}\,\theta\,\mathrm{c}\,\psi \\ -\mathrm{s}\,\theta & \mathrm{c}\,\theta\,\mathrm{s}\,\psi & \mathrm{c}\,\theta\,\mathrm{c}\,\psi \end{bmatrix}$$

with the following differential kinematics:

$$\begin{pmatrix} \dot{\phi} \\ \dot{\theta} \\ \dot{\psi} \end{pmatrix} = \frac{1}{\mathrm{c}\,\theta} \begin{bmatrix} 0 & \mathrm{s}\,\psi & \mathrm{c}\,\psi \\ 0 & \mathrm{c}\,\theta\,\mathrm{c}\,\psi & -\mathrm{c}\,\theta\,\mathrm{s}\,\psi \\ \mathrm{c}\,\theta & \mathrm{s}\,\theta\,\mathrm{s}\,\psi & \mathrm{s}\,\theta\,\mathrm{c}\,\psi \end{bmatrix} \omega_o \tag{42}$$

and

$$r_e^w = R_o e_1 = \begin{bmatrix} \mathrm{c}\,\phi\,\mathrm{c}\,\theta & \mathrm{s}\,\phi\,\mathrm{c}\,\theta & -\mathrm{s}\,\theta \end{bmatrix}^T$$

where $|\theta| < \pi/2$ and $\mathrm{s}\star = \sin\star$, $\mathrm{c}\star = \cos\star$. Note here that r_e^w is a function of only (ϕ, θ).

Following the explanation above on $\Delta_u \nu_u$ with (16), we have $\omega_o = [\Delta_u \nu_u; 0; 0] + A\nu_a$, and, injecting this into (42), we can write:

$$\dot{\psi} = ||d_2 - d_1|| \cdot \nu_u + A\nu_a$$

where $A \in \Re^{6\times 5}$ is a function of the configuration (x_e, R_o). Incorporating this $\dot{\psi}$ into (41) while also writing g_u with $[\phi, \theta, \psi]$, we can then write the internal dynamics (41) s.t.,

$$\begin{aligned} m_u \ddot{\psi} + \bar{m} g ||d_1 \times d_2|| \,\mathrm{c}\,\theta\,\mathrm{s}\,\phi \\ = m_u \cdot [\nabla A(\nu_a, \nu_u)\nu_a + A\dot{\nu}_a] - C_{ua}\nu_a + f_u \end{aligned} \tag{43}$$

where $m_u := M_u / ||d_2 - d_1|| > 0$ and $\nabla A(\xi)$ and $C_{ua}(\xi)$ are linear in ν_a and ν_u. We can then see that the internal dynamics (43) is indeed similar to the downward pendulum dynamics, suggesting that, if the perturbation (i.e., $\nu_a, \dot{\nu}_a, f_u$) is small enough, it would be stable with bounded $\psi, \dot{\psi}$ as formalized in the next Lem. 1.

Lemma 1. *Consider the internal dynamics* (43) *and assume the followings: 1) the tracking control* u_a (37) *is designed slow enough with* $||\nu_a||, ||\dot{\nu}_a||$ *bounded; 2)* $f_u \in \Re$ *is bounded; and 3) there is unmodeled/physical damping* $-b_u\dot{\psi}$ *for* (43)*. Then, there always exists small enough* $\bar{\nu}_a \geq 0$*,* $||\nu_a(t)|| \leq \bar{\nu}_a$*,* $\forall t \geq 0$*, such that* $(\psi(t), \dot{\psi}(t))$ *is bounded* $\forall t \geq 0$*.*

Proof. Incorporating the physical/unmodeled damping b_u and also linearizing the internal dynamics (43) around $(\psi, \dot{\psi}) = 0$, we can obtain:

$$m_u \ddot{\psi} + b_u \dot{\psi} + k_u \,\mathrm{c}\,\theta \cdot \psi = g_1(\nu_a, \nu_u)\nu_a + g_2 \dot{\nu}_a + f_u$$

where $k_u := \bar{m} g ||d_1 \times d_2||$, $g_1 \in \Re^{1\times 5}$ is linear in its arguments, $g_2 \in \Re^{1\times 5}$ is bounded, and the terms in RHS (right hand side) are all bounded, if so is ν_u.

Define the following Lyapunov function:

$$V_u := \frac{1}{2} m_u \dot{\psi}^2 + \epsilon \psi \dot{\psi} + \frac{1}{2} \,\mathrm{c}\,\theta \psi^2$$

where $\epsilon > 0$ is a cross-coupling term [11] chosen s.t., (i) $\epsilon < \sqrt{m_u \,\mathrm{c}\,\theta}$ to ensure V_u be positive-definite. Differentiating this V_u along the above internal dynamics, we can then obtain:

$$\begin{aligned} \dot{V}_u = \begin{pmatrix} \dot{\psi} \\ \psi \end{pmatrix}^T \begin{bmatrix} b_u - \epsilon & \frac{1}{2} b_u \epsilon \\ \frac{1}{2} b_u \epsilon & \epsilon \,\mathrm{c}\,\theta + \frac{1}{2} \,\mathrm{s}\,\theta \cdot \dot{\theta} \end{bmatrix} \begin{pmatrix} \dot{\psi} \\ \psi \end{pmatrix} \\ + (g_1(\nu_a, \nu_u)\nu_a + g_2 \dot{\nu}_a + f_u) \cdot (\dot{\psi} + \epsilon\phi) \end{aligned}$$

where the first term in RHS will be negative-definite if: (ii) $b_u - \epsilon > 0$; (iii) $\epsilon > \frac{1}{2} |\tan\theta| \cdot |\dot{\theta}|$; and (iv) $(b_u - \epsilon)(\epsilon \,\mathrm{c}\,\theta + \frac{1}{2} \,\mathrm{s}\,\theta\dot{\theta}) > \frac{1}{4} b_u^2 \epsilon^2$. The solution ϵ of the inequalities (i)-(iii) is then given by

$$\tfrac{1}{2} |\tan\theta| \cdot |\dot{\theta}| < \epsilon < \min(\sqrt{m_u \,\mathrm{c}\,\theta}, b_u)$$

which will always have an intersection with the solution of (iv), i.e., $\epsilon \geq 0$ s.t.,

$$\left(\tfrac{1}{4} b_u^2 + \mathrm{c}\,\theta\right) \epsilon^2 - (b_u \,\mathrm{c}\,\theta - \eta)\epsilon + b_u \eta < 0$$

as $|\dot{\theta}| \leq \bar{\nu}_a \to 0$, where $\eta := \frac{1}{2} \,\mathrm{s}\,\theta \cdot \dot{\theta} \to 0$ as well with $\bar{\nu}_a \to 0$. This then means that, with small enough $\bar{\nu}_a$, V_u will always be positive-definite with $\dot{V}_u \leq -\alpha_1 V_u + \alpha_2 \sqrt{V_u}$ for some $\alpha_1, \alpha_2 > 0$, implying the boundedness of $(\psi(t), \dot{\psi}(t))$ $\forall t \geq 0$. □

Note that the physical/unmodeled damping b_u assumed in Lem. 1 in general exists in the real systems (e.g., aero-dynamic dissipation). This physical damping would also perturb the tracking control objective of Th. 2, whose effect yet can be adequately reduced by increasing the feedback gains k_ν, k_x, k_r of (37) during our experimentations - see Sec. VI. The assumption of f_u being bounded would also be likely granted in practice for the S2Q-platform system of Fig. 3, since it denotes the reaction moment along the N^E-axis exerted only at the tool-tip with the moment-arm length being the radius of tool-tip itself.

C. Optimal Control Allocation and Closed-Form Expression

Given the desired control wrench $U = \Omega_a^T u_a$ in (31) with u_a in (37) and $u_u = 0$, the next task is to allocate this $U =: [u_f, u_\tau]$ into the thrust of each quadrotor Λ_i^o of the S2Q-platform of Fig. 3 via the constrained optimization (9)-(12). Existence of solution of this allocation problem is assumed by designing the task to be control feasible as stated in Sec. III-B. Further, as shown below, for the S2Q-platform system of Fig. 3, we can in fact find a closed-form expression of the optimization problem (9)-(12), eliminating the necessity of relying on iterative procedures as for the S3Q-platform system in Sec. IV-B.

For this, similar to Sec. IV-B, we reduce the size of the optimization problem (9)-(12) by utilizing the control generation equation (10), which can be rewritten as

$$\begin{bmatrix} I & I \\ 0 & S(d_2 - d_1) \end{bmatrix} \Lambda = \begin{pmatrix} u_f \\ -S(d_1)u_f + u_\tau \end{pmatrix} \tag{44}$$

by multiplying both sides of (10) with

$$\begin{bmatrix} I & 0 \\ -S(d_1) & I \end{bmatrix}$$

This matrix is the transpose of the adjoint operator, mapping $U = (u_f, u_\tau)$ expressed in $\{\mathcal{F}_O\}$ attached at x_c to its equivalent wrench expressed in $\{\mathcal{F}_1\}$ attached at x_1 with the same attitude as $\{\mathcal{F}_O\}$. Note that this adjoint operator also appears in (16).

Denote the general solution of (44) by $\bar{\Lambda} = [\bar{\Lambda}_1; \bar{\Lambda}_2]$ with $\bar{\Lambda}_i := [\bar{\lambda}_{i_1}; \bar{\lambda}_{i_2}; \bar{\lambda}_{i_3}] \in \Re^3$. We can then easily determine $\bar{\lambda}_{2_2}$ and $\bar{\lambda}_{2_3}$ from (44) s.t.,

$$\bar{\lambda}_{2_2} = \frac{1}{\|d_2 - d_1\|} e_3^T [-S(d_1)u_f + u_\tau]$$
$$\bar{\lambda}_{2_3} = -\frac{1}{\|d_2 - d_1\|} e_2^T [-S(d_1)u_f + u_\tau]$$

and, further, compute $\bar{\lambda}_{1_2}, \bar{\lambda}_{1_3}$ s.t.,

$$\bar{\lambda}_{1_2} = e_2^T u_f - \bar{\lambda}_{2_2}, \quad \bar{\lambda}_{1_3} = e_3^T u_f - \bar{\lambda}_{2_3}$$

Recall from (15) that the rank of the first matrix in LHS (left hand side) of (44) is five. This then means that the solution of (44) assumes one-dimensional null-space, which can be obtained by using the first row of (44), i.e.,

$$\bar{\lambda}_{1_1} = \tfrac{1}{2} u_{f_1} + \gamma, \quad \bar{\lambda}_{2_1} = \tfrac{1}{2} u_{f_1} - \gamma$$

where $u_f =: [u_{f_1}; u_{f_2}; u_{f_3}] \in \Re^3$ and $\gamma \in \Re$ identifies the null-space.

Substituting these $\bar{\Lambda}_1, \bar{\Lambda}_2 \in \Re^3$ into (9)-(12), we can obtain the reduced form of the constrained optimization problem w.r.t. $\gamma \in \Re$ s.t.,

$$\gamma_{\text{op}} = \arg\min_{\gamma \in \Re} \gamma^2 + \frac{1}{2} \left[u_{f_1}^2 + \sum_{i=1}^{2} (\bar{\lambda}_{i_2}^2 + \bar{\lambda}_{i_3}^2) \right] \tag{45}$$

subject to

$$-a_1 \le \tfrac{1}{2} u_{f_1} + \gamma \le a_1, \quad -b_1 \le \tfrac{1}{2} u_{f_1} + \gamma \le b_1$$
$$-a_2 \le \tfrac{1}{2} u_{f_1} - \gamma \le a_2, \quad -b_2 \le \tfrac{1}{2} u_{f_1} - \gamma \le b_2$$

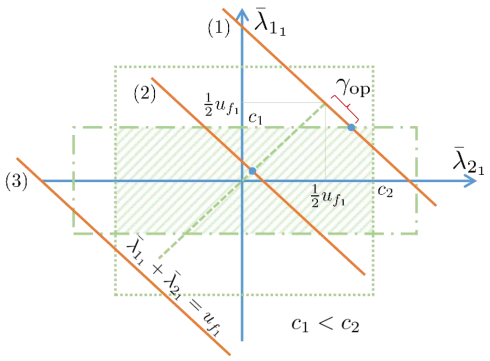

Fig. 5: Geometry of the reduced optimization problem (45) with transversing anchoring point $(\frac{1}{2}u_{f_1}, \frac{1}{2}u_{f_1})$ and the shaded feasible region: (1) solution exists with non-zero γ_{op}; (2) solution exists with $\gamma_{\text{op}} = 0$; and (3) no solution exists for γ_{op}.

where

$$a_i := \sqrt{\tfrac{1-\cos^2\phi_i}{\cos^2\phi_i} \bar{\lambda}_{i_3}^2 - \bar{\lambda}_{i_2}^2}, \quad b_i := \sqrt{\bar{\lambda}_i^2 - \bar{\lambda}_{i_2}^2 - \bar{\lambda}_{i_3}^2}$$

are to be positive constants when the control feasibility condition of Prop. 2 is enforced by the task design.

Define $c_i := \min(a_i, b_i)$. Note also that the last term in RHS of (45) is a constant, thus, can be simply dropped off. We can then think of the geometry of this reduced constrained optimization problem w.r.t. γ as illustrated in Fig. 5, where the anchoring point $(\bar{\lambda}_{1_1}, \bar{\lambda}_{2_1}) = \frac{1}{2}(u_{f_1}, u_{f_1})$ is transversing according to a given u_{f_1} and a solution exists when the slant line intersects with the shaded feasible region. From this Fig. 5, we can obtain the following closed-form solution:

$$\gamma_{\text{op}} = \begin{cases} 0 & \text{if } \frac{1}{2}|u_{f_1}| \le \min(c_1, c_2) \\ \frac{1}{2}u_{f_1} - c_2 & \text{if } \frac{1}{2}|u_{f_1}| > \min(c_1, c_2) \text{ and } c_1 \ge c_2 \\ -\frac{1}{2}u_{f_1} + c_1 & \text{if } \frac{1}{2}|u_{f_1}| > \min(c_1, c_2) \text{ and } c_1 < c_2 \end{cases}$$

No solution γ_{op} exists when $|u_{f_1}| > |c_1 + c_2|$, which however is ruled out here by enforcing the control feasibility of Prop. 2.

VI. Experimental Results

A. Setup

We build the prototypes of S3Q-platform and S2Q-platform using AscTec Hummingbird quadrotors connecting to a frame using passive spherical joints. The frames are constructed of lightweight carbon fiber. The geometry of the prototypes are shown in Fig. 1 and Fig. 3 with the following geometric design parameter: $\|d_i - d_j\| = 1$ [m], and $(d_i - d_j)^T e_3 = 0$. The spherical joints allow the range of angle motion $\phi_i = 32^\circ$ and be arranged aligned with the D^o-axis to maximize the system payload (i.e., $p_i = e_3$). We locate the spherical joints close to the quadrotor center-of-masses (see Fig. 3) to satisfy the assumption in Sec. II as much as we can. Some important specifications of these prototypes are given in Table I.

We here use AscTec Hummingbird quadrotors with its weight of 0.6 [kg] and recommended payload of 0.2 [kg]. In our experiments, the maximum payload the quadrotor can carry is 0.6 [kg], equivalent to the maximum thrust of 11.8

Prototype	System weight	Payload	Horizontal force
S2Q-platform	1.54 [kg]	0.7 [kg]	14 [N]
S3Q-platform	2.31 [kg]	1.2 [kg]	20 [N]

TABLE I: Parameters and specifications of S2Q-platform and S3Q-platform prototypes.

[N]. The quadrotors are embedded with the attitude controller running onboard and receiving roll and pitch angles, yaw rate and the throttle as the quadrotor input command. We compute the input command on a remote PC and send it to the quadrotors via XBee communication. We use the motion capture system (MOCAP: VICON®) to measure the attitude of quadrotors and the position and attitude of the frame. To deal with the problem of noisy angular rate measurements with MOCAP, we employ a low-pass filter, in which the filter gains are tuned by comparing the measurements using IMU and MOCAP. We then need to translate the desired thrust Λ_i given in Sec. IV and Sec. V into each rotor command of the quadrotors. There are many techniques available to control the quadrotors to track that desired Λ_i. For the S2Q-platform, we use the backstepping control [34] to provide a good performance since we have the explicit expression of the thrust Λ_i and its derivative for S2Q-platform. For S3Q system, where the thrust Λ_i are determined numerically, we employ a method that computes the quadrotor commands directly from the thrust Λ_i - see Appendix B.

B. Control of S3Q-Platform Prototype

To evaluate the performance of the prototype, we first perform the hovering experiment. The results are shown in Fig. 6. For comparison, we also include the hovering results of a single AscTec Hummingbird quadrotor. From Fig. 6 and Fig. 7, we can see that the performance of the S3Q platform (i.e., RMS error of 2.3 [cm] in position and 2.2^o in attitude), despite its high system complexity, is still comparable to that of the well-built AscTec Hummingbird quadrotor (i.e., RMS error of 1.4 [cm] and 0.9^o).

We now consider the motion tracking control of S3Q-platform, which requires the center-of-mass of the frame $x_e^w = x_o^w$ to track a horizontal rectangular shape while maintaining the platform hovering posture (i.e., $R_d \approx I_{3\times3}$). The desired motion is designed to be feasible according to the task planning procedure in Sec. III-B - see Fig. 4. The results are shown in Fig. 8a, where we see that the frame center-of-mass tracks the desired motion with the RMS position error of 4.6 [cm] while maintaining the hovering attitude with the RMS angle error of 4.2^o.

To examine the compliant/backdrivable interaction capability of the S3Q system, we stabilize the system in the hovering posture at a fixed position ($x_o^w \to [0; 0; 1.5]$ [m]) and apply some external wrenches to that in N^o, E^o, D^o directions at different positions, as shown in the snapshot of Fig. 8b. The pose deviation from the hovering pose is proportional to the external wrenches. Fig. 8b depicts the response of the system during the interaction with the markings $(1), (2), (3), (4), (5)$ corresponding to the platform response at five instances $t \in$

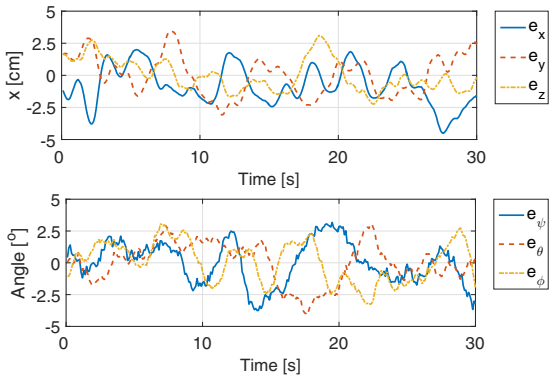

Fig. 6: S3Q-platform hovering with RMS errors of 2.3 [cm] in position and 2.2^o in attitude.

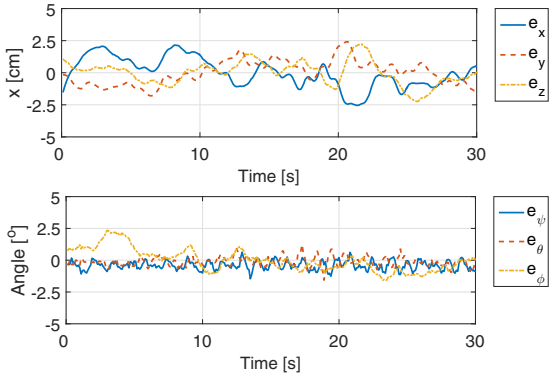

Fig. 7: Quadrotor hovering with RMS errors of 1.4 [cm] in position and 0.9^o in attitude.

$\{4, 7, 12, 15, 21\}$ [s]. In this experiment, we give high stiff gain k_r on the attitude error, which gives higher priority to maintaining the attitude of the frame. We can see that under the external wrench at the instance (4) and (5), the position of the frame change accordingly, i.e., position error of 0.14 [m] in the z-axis, while the attitude error is fairly small with 8^o at (4) and 10^o at (5) since this given external wrench can be compensated for by the combination of the torque about E^o, N^o axes and the force along D^o axis. Compare to Sec. VI-C, where higher priority is given to maintaining the position. We can see that the attitude and position error of the system are bounded under this external wrench, and when the external wrench is removed, the S3Q-frame recovers to its hovering pose/position. Here, note that this compliant interaction is attained with no force/torque sensors, clearly showing that the SmQ system is backdrivable. Recall that, depending on the location of the tool-tip, direct interaction with standard quadrotors can be unstable due to their internal dynamics stemming from the under-actuation [35]. In contrast to that, here, regardless of the contact location (e.g., tool-tip shape), the interaction stability is guaranteed due to the full-actuation of the S3Q system in SE(3).

The combination of the precise motion tracking and compliant interaction capability makes the S3Q-platform suitable for aerial manipulation. One such example would be tele-mapulating an object using haptic device. The results are shown in Fig. 8c, where we can see that the system follows precisely the desired command (i.e., position tracking RMS

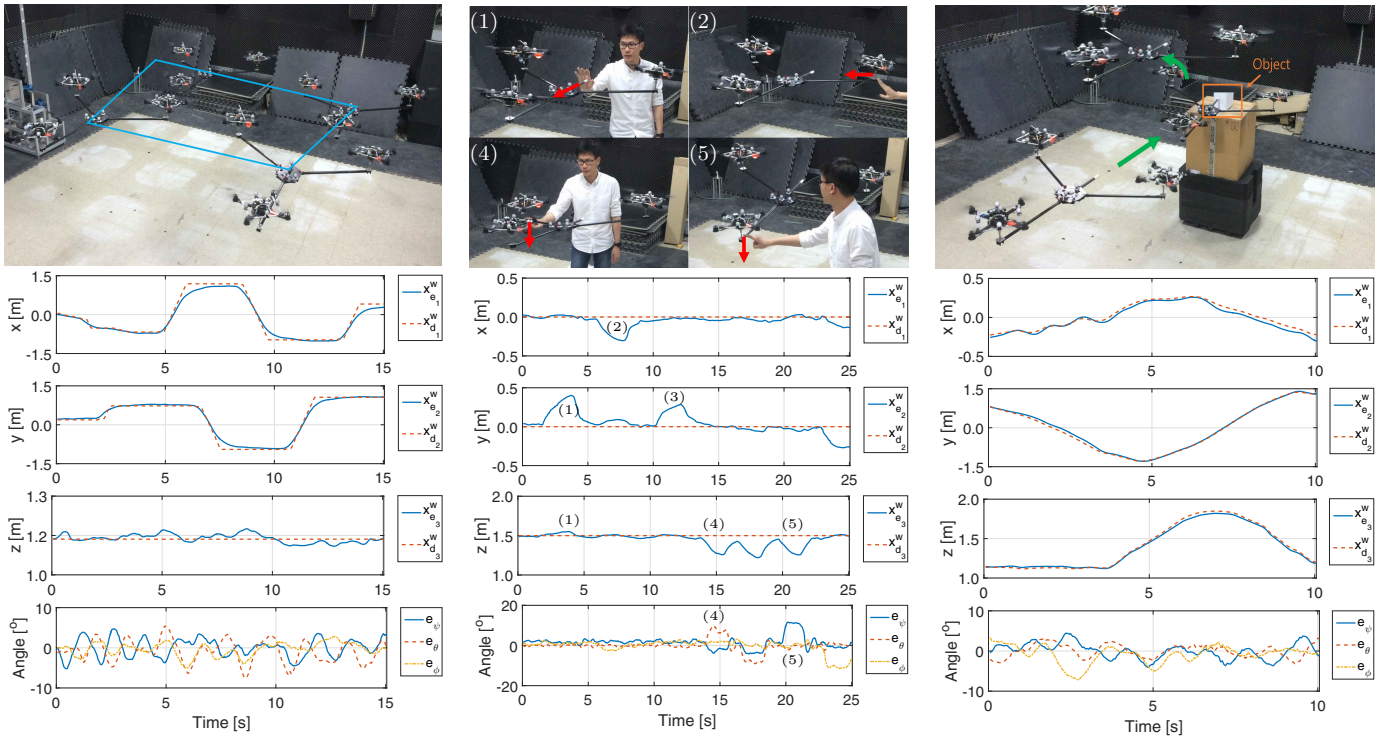

(a) Trajectory tracking: center-of-mass of the S3Q-frame tracking a horizontal rectangular shape while maintaining hovering posture (i.e., $R_o \approx I_{3\times 3}$).

(b) Stable interaction: position and attitude of the S3Q-frame response to the external wrench applied to the frame at $t \in \{4, 7, 12, 15, 21\}$ [s].

(c) Manipulation task: tele-manipulating an object using haptic device.

Fig. 8: Experiments of S3Q-platform prototype.

error of 4.7 [cm] and attitude RMS error of 2.6^o) from the user while compliantly interacting with the environment. [3]

C. Control of S2Q-Platform Prototype

Similar to Sec. VI-B, we perform the motion control experiment of the S2Q system, i.e., the tool-tip position tracking of a horizontal circular shape while maintaining a certain pointing direction (e.g., pitch at zero and yaw at 45^o). This task is designed to be feasible according to the task-planning in Sec. III-B - see Fig. 4a. The results are shown in Fig. 9a, where we can see that the S2Q-platform can track this feasible motion with the tracking RMS error of 2.7 [cm] while maintaining the desired pointing direction (i.e., yaw and pitch angles with RMS error of 5.6^o). Since this task requires purely motion tracking, we adopt a virtual tool-tip located on the line connecting the center-of-mass of two quadrotors and utilize the control designed in Sec. V.

Fig. 9b shows the results of the interaction experiment with the S2Q platform through its tool-tip. For this, we utilize a physical tool with the tool-tip located on the line connecting the two quadrotors, i.e., satisfying the condition (17). See Fig. 9b. We can see that the point-contact force at the tool-tip does not create external torque on the un-actuated direction of S2Q system. In this task we perform stabilization with the geometric center point of two quadrotors $x_e = \frac{1}{2}(x_1 + x_2) \to [0; 0; 1.5]$ [m]. We then apply point-contact forces at the tool-tip along N^o, E^o, D^o directions. Fig. 9b presents the response of the system to the interaction wrench with the markings $(1), (2), (3)$ corresponding to the responses at instances $t \in \{8, 20, 32\}$ [s]. We then see that the contact force along N^o direction causes a proportional position error in e_1 axis. With the contact force along E^o, D^o directions at the physical tool-tip, i.e., instances $(2), (3)$, the system can generate counter-acting force along E^o, D^o directions at x_e^o and counter-acting torque about D^o, E^o directions. In this implementation, we give higher priority to maintaining the position x_e^o by using high stiff gain k_x. Thus, the attitude errors change accordingly while the position errors remain fairly small. See the marking points $(2), (3)$ on Fig. 9b.

We also perform a tele-operation tasks, i.e., using a haptic device to remotely control the tool-tip to push a box of 3×4.5 [cm]. As expected, the tool-tip tracks the desired motion generated by the haptic device with RMS error of 3.0 [cm] and 3.2^o and we can accomplish the task - see Fig. 9c. In all these tasks, the S2Q system exhibits some roll motion. However, as expected, the roll angle remains bounded in all tasks with the RMS error of 1.4^o in the circular motion, 1.2^o in the interaction task and 1.5^o in the teleoperation task, which confirms the boundedness of the un-actuated dynamic in Lemma 1. See Fig. 9.[4]

[3] Experiment video of S3Q platform prototype can be found at https://youtu.be/FTVTytxRoEo

[4] Experiment video of S2Q platform prototype can be found at https://youtu.be/uBC6aEII-0o

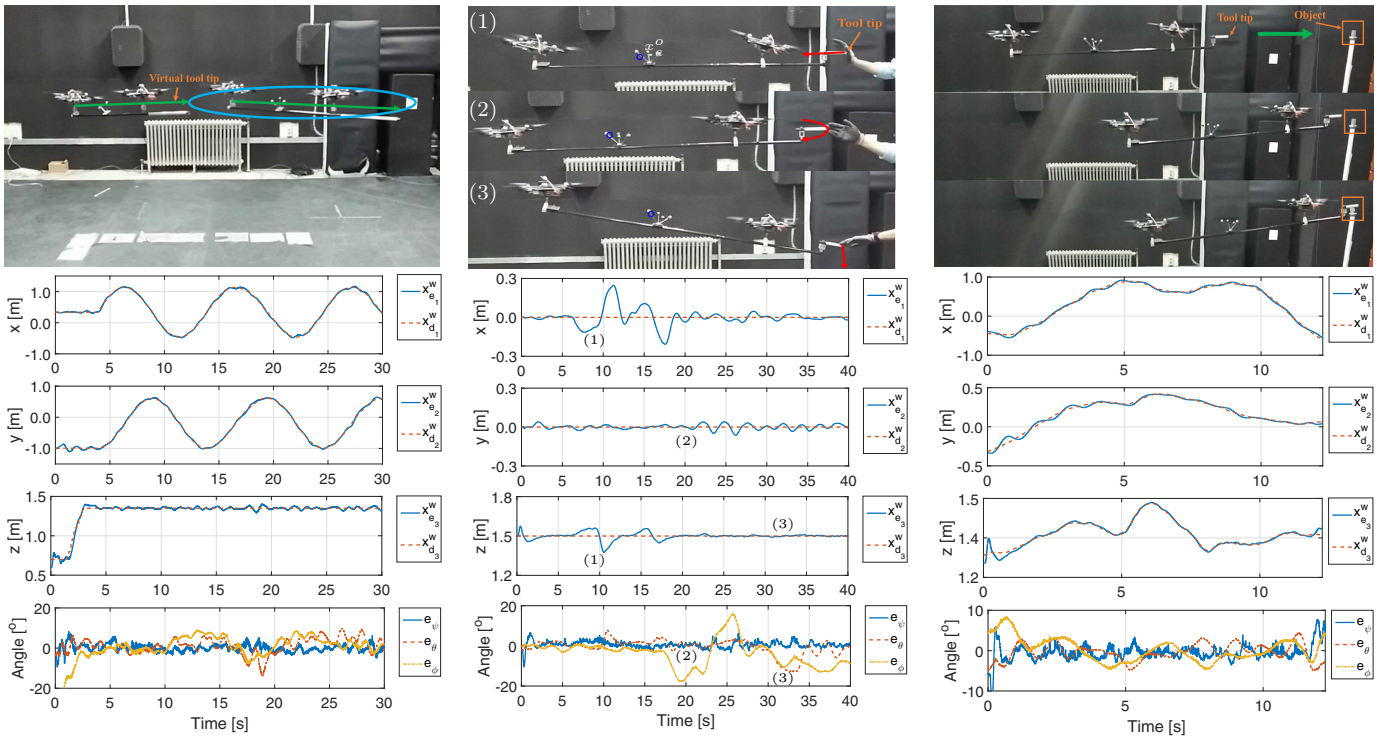

(a) Trajectory tracking: the virtual tool-tip on the line connecting the center-of-mass positions of two quadrotors tracking a horizontal circular shape while maintaining a certain attitude (e.g., pitch at zero and yaw at 45^o).

(b) Stable interaction: geometric center point x_e and the pointing direction of S2Q-platform under the external wrench applied to the frame at $t \in \{8, 20, 32\}$ [s].

(c) Manipulation task: tele-manipulating an object of 3×4.5 [cm] using haptic device.

Fig. 9: Experiments of S2Q-platform prototype.

VII. Conclusion

In this paper, we presented a novel aerial manipulation platform, SmQ (spherically-connected multi-quadrotor) platform, which consists of multiple quadrotors connected to a frame through passive spherical joints. This proposed SmQ platform can overcome the well-known issues of under-actuation of multi-rotor drones for aerial operation/manipulation, allowing for more robust operation (particularly against side-way forcing/gust), dynamic control for faster/smoother interaction, and simpler/modular integration with a multi-DOF robotic arm, as compared to systems based on the conventional multi-rotor drones. In this paper, we provide theoretical framework for this SmQ platform system, particularly, for its modeling and control, while also elucidating issues related to: 1) how to design the SmQ systems to be fully-actuated in SE(3); 2) how to attain closed-loop control of the SmQ system while respecting such physical constraints as the range limit of the spherical joints and the thrust saturations. The performance and possible utility of the SmQ system are also demonstrated via experiments for various scenarios, encompassing from motion control and simple mechanical operation to impedance interaction control and tele-manipulation.

Some topics for future work include: 1) optimal motion planning of SmQ system with its dynamics, constraints and uncertainty incorporated; 2) implementation of the SmQ system with only onboard sensing and computing; and 3) integration of the SmQ system with multi-DOF robotic arm and different types of drones (e.g., three rotors).

References

[1] C. Korpela, M. Orsag, M. Pekala, and P. Oh. Dynamic stability of a mobile manipulating unmanned aerial vehicle. In *Proc. IEEE Int'l Conference on Robotics and Automation*, pages 4922–4927, 2013.

[2] S. Kim, S. Choi, and H. J. Kim. Aerial manipulation using a quadrotor with a two dof robotic arm. In *Proc. IEEE/RSJ Int'l Conference on Intelligent Robots and Systems*, pages 4990–4995, 2013.

[3] A. E. Jimenez-Cano, J. Martin, G. Heredia, A. Ollero, and R. Cano. Control of an aerial robot with multi-link arm for assembly tasks. In *Proc. IEEE Int'l Conference on Robotics and Automation*, pages 4916–4921, 2013.

[4] J. Scholten, M. Fumagalli, S. Stramigioli, and R. Carloni. Interaction control of an UAV endowed with a manipulator. In *Proc. IEEE Int'l Conference on Robotics and Automation*, pages 4910–4915, 2013.

[5] H. Yang and D. J. Lee. Dynamics and control of quadrotor with robotic manipulator. In *Proc. IEEE Int'l Conference on Robotics & Automation*, pages 5544–5549, 2014.

[6] G. Garimella and M. Kobilarov. Towards model-predictive control for aerial pick-and-place. In *Proc. IEEE Int'l Conference on Robotics and Automation*, pages 4692–4697, 2015.

[7] M. Kamel, K. Alexis, and R. Siegwart. Design and modeling of dexterous aerial manipulator. In *Proc. IEEE/RSJ Int'l Conference on Intelligent Robots and Systems*, pages 4870–4876, 2016.

[8] H. Lee and H. J. Kim. Estimation, control, and planning for autonomous aerial transportation. *IEEE Transactions on Industrial Electronics*, 64(4):3369–3379, 2017.

[9] M. Orsag, C. Korpela, S. Bogdan, and P. Oh. Dexterous aerial robots Mobile manipulation using unmanned aerial systems. *IEEE Transactions on Robotics*, 33(6):1453–1466, 2017.

[10] F. Bullo and K. Lynch. Kinematic controllability for decoupled trajectory planning in underactuated mechanical systems. *IEEE Transactions on Robotics & Automation*, 17(4):402–412, 2001.

[11] R. M. Murray, Z. Li, and S. S. Sastry. *A Mathematical Introduction to Robotic Manipulation*. CRC Press, 1994.

[12] G. Jiang and R. Voyles. A nonparallel hexrotor UAV with faster response to disturbances for precision position keeping. In *Proc. IEEE Int'l Symposium on Safety, Security, and Rescue Robotics*, pages 1–5, 2014.

[13] S. Rajappa, M. Ryll, H. H. Bulthoff, and A. Franchi. Modeling, control and design optimization for a fully-actuated hexarotor aerial vehicle with tilted propellers. In *Proc. IEEE Int'l Conference on Robotics and Automation*, pages 4006–4013, 2015.

[14] A. Nikou, G. C. Gavridis, and K. J. Kyriakopoulos. Mechanical design, modelling and control of a novel aerial manipulator. In *Proc. IEEE Int'l Conference on Robotics and Automation*, pages 4698–4703, 2015.

[15] D. Brescianini and R. D'Andrea. Design, modeling and control of an omni-directional aerial vehicle. In *Proc. IEEE Int'l Conference on Robotics and Automation*, pages 3261–3266, 2016.

[16] S. Park, J. Her, J. Kim, and D. J. Lee. Design, modeling and control of omni-directional aerial robot. In *Proc. IEEE/RSJ Int'l Conference on Intelligent Robots and Systems*, pages 1570–1575, 2016.

[17] M. Ryll, H. H. Bulthoff, and P. R. Giordano. A novel overactuated quadrotor unmanned aerial vehicle: Modeling, control, and experimental validation. *IEEE Transactions on Control Systems Technology*, 23(2):540–556, 2015.

[18] M-D. Hua, T. Hamel, and C. Samson. Control of VTOL vehicles with thrust-tilting augmentation. *Automatica*, 52:1–7, 2015.

[19] A. Oosedo, S. Abiko, S. Narasaki, A. Kuno, A. Konno, and M. Uchiyama. Flight control systems of a quad tilt rotor unmanned aerial vehicle for a large attitude change. In *Proc. IEEE/RSJ Int'l Conference on Intelligent Robots and Systems*, pages 2326–2331, 2015.

[20] M. Ryll, D. Bicego, and A. Franchi. Modeling and control of FAST-Hex: A fully-actuated by synchronized-tilting hexarotor. In *Proc. IEEE/RSJ Int'l Conference on Intelligent Robots and System*, pages 1689–1694, 2016.

[21] R. Oung and R. D'Andrea. The distributed flight array. *Mechatronics*, 21:908–917, 2011.

[22] D. Mellinger, M. Shomin, N. Michael, and V. Kumar. *Cooperative Grasping and Transport Using Multiple Quadrotors*, volume 83 of *Springer Tracts in Advanced Robotics*, chapter 39, pages 545–558. Springer Berlin Heidelberg, 2013.

[23] N. Michael, J. Fink, and V. Kumar. Cooperative manipulation and transportation with aerial robots. In *Proc. Robotics: Science and Systems*, 2009.

[24] K. Sreenath and V. Kumar. Dynamics, control and planning for cooperative manipulation of payloads suspended by cables from multiple quadrotor robots. In *Proc. Robotics: Science and Systems*, 2013.

[25] M. Manubens, D. Devaurs, L. Ros, and J. Cortes. Motion planning for 6d manipulation with aerial towed-cable systems. In *Proc. Robotics: Science and Systems*, 2013.

[26] H-N. Nguyen, S. Park, and D. J. Lee. Aerial tool operation system using quadrotors as rotating thrust generators. In *Proc. IEEE/RSJ Int'l Conference on Intelligent Robots and Systems*, pages 1285–1291, 2015.

[27] S. P. Boyd and L. Vandenberghe. *Convex Optimization*. Cambridge University Press, 2009.

[28] A. V Fiacco and Y. Ishizuka. Sensitivity and stability analysis for nonlinear programming. *Annals of Operations Research*, 27(1):215–235, 1990.

[29] J-W. Li, H. Liu, and H-G. Cai. On computing three-finger force-closure grasps of 2-D and 3-D objects. *IEEE Transactions on Robotics and Automation*, 19(1):155–161, 2003.

[30] N. A. Chaturvedi, A. K. Sanyal, and N. H. McClamroch. Rigid-body attitude control. *IEEE Control Systems Magazine*, 31(3):30–51, 2011.

[31] T. Lee. Global Exponential Attitude Tracking Controls on SO(3). *IEEE Transactions on Automatic Control*, 60(10):2837–2842, 2015.

[32] M. W. Spong, S. Hutchinson, and M. Vidyasagar. *Robot Modeling and Control*. John Wiley & Son, 2006.

[33] D. J. Lee and P. Y. Li. Passive decomposition of mechanical systems with coordination requirement. *IEEE Transactions on Automatic Control*, 58(1):230–235, 2013.

[34] C. Ha, Z. Zuo, F. B. Choi, and D. J. Lee. Passivity-based adaptive backstepping control of quadrotor-type UAVs. *Robotics and Autonomous Systems*, 62(9):1305–1315, 2014.

[35] H-N. Nguyen, C. Ha, and D. J. Lee. Mechanics, control and internal dynamics of quadrotor tool operation. *Automatica*, 61:289–301, 2015.

APPENDIX

A. Notations

Notation	Description
$\mathcal{F}_W$	Inertial world frame
$\mathcal{F}_0, \mathcal{F}_i$	Body frame of SmQ-frame and quadrotor i
$n \in \mathbb{N}^+$	Number of quadrotors of the system
$m_o, m_i \in \Re$	Mass of the SmQ-frame and the quadrotor i
$J_o, J_i \in \Re$	Inertia of the SmQ-frame and the quadrotor i
$x_o^w, x_i^w \in \Re^3$	CoM positions of SmQ-frame and quadrotor i
$R_o, R_i \in$ SO(3)	Attitudes of SmQ-frame and quadrotor i
$v_i := R_i^T \dot{x}_i^w$	Translation velocity in the body-fixed frame
$\omega_o, \omega_i \in \mathfrak{so}(3)$	Angular velocities in the body-fixed frames
$x_c^w, v_c^0 \in \Re^3$	Position/velocity of system CoM (See (5))
$\xi := [v_c; \omega_o] \in \Re^6$	Translation/angular velocities of system CoM
$d_i := x_i - x_c$	Position of quadrotor i w.r.t. system CoM
$\Lambda_i^0 \in \Re^3$	Thrust vector of quadrotor i in $\mathcal{F}_0$
$\lambda_i \in \Re, \lambda_i \leq \bar{\lambda}_i$	Thrust magnitude of quadrotor i, and its bound
$N_i^w \in \Re^3$	Constraint between SmQ-frame and quadrotor i
$p_i^o \in \Re^3$	Center axis of the i-th spherical joint
$\phi_i \in \Re$	Motion range of spherical joint i
$f_e^o, \tau_e^o \in \Re^3$	External force/torque at CoM of SmQ-frame
$S(\omega) \in \Re^{3\times 3}$	$S(\omega)\nu = \omega \times \nu, \forall \omega, \nu \in \Re^3$

B. Quadrotor Thrust Decode

In Sec. IV and Sec. V, the required thrust vector Λ_i are computed for each quadrotor. Here, we explain how to compute the rotor commands from this desired thrust vector Λ_i for the quadrotor. Let us parameterize $R_i \in SO(3)$ of the i-th quadrotor using yaw, pitch, roll angles $\eta_i := [\phi_i; \theta_i; \psi_i] \in \Re^3$, that is, $R_i(\eta) = R_{e_3}(\phi_i) R_{e_2}(\theta) R_{e_1}(\psi)$, with $R_{e_i}(\star)$ being the elementary rotation matrix about the e_i-axis [32]. The objective is then computing the throttle $|\lambda_i|$ and attitude command (ψ_i, θ_i) such that

$$\lambda_i R_i(\eta) e_3 = R_o \Lambda_i \tag{46}$$

where ψ_i can be arbitrary. We now rewrite (46) as

$$\lambda_i R_{e_2}(\theta) R_{e_1}(\psi) e_3 = R_{e_3}^T(\phi_i) R_o \Lambda_i$$

We choose the throttle command $|\lambda_i| = \|\Lambda_i\|$ and the attitude command such that

$$\begin{bmatrix} \sin\theta_i \cos\psi_i \\ -\sin\phi_i \\ \cos\theta_i \cos\psi_i \end{bmatrix} = \frac{1}{\|\Lambda_i\|} R_{e_3}^T(\phi_i) \Lambda_i =: \hat{\Lambda}_i(\psi_i) \in \Re^3.$$

This suggests to choose the roll and pitch commands as

$$\psi_i = -\sin^{-1} \hat{\Lambda}_{i_2}, \qquad \theta_i = \tan^{-1} \frac{\hat{\Lambda}_{i_1}}{\hat{\Lambda}_{i_3}}.$$

Hai-Nguyen Nguyen (S'14) received his B.S. degree in Mechatronics and his M.S. degree in Engineering Mechanics from the Hanoi University of Science & Technology, Vietnam, 2008 and 2010. From 2009 to 2012, he was a permanent researcher with the Institute of Mechanics, Vietnam Academy of Science & Technology. He is currently working toward a Ph.D. degree in Mechanical Engineering at Seoul National University. His research interests include dynamics and control problems related to aerial manipulation.

Sangyul Park (S'15) received his B.S. degree in Mechanical & Aerospace Engineering from the Seoul National University, Seoul, Korea, 2013. He is currently working toward a Ph.D. degree in Mechanical Engineering at the Seoul National University. His research interests include design, modeling and control of new aerial robotic systems.

Junyoung Park (S'17) received his B.S. degree in Mechanical Engineering from Pohang University of Science and Technology in 2016. He is currently working toward his M.S. degree in Mechanical Engineering at Seoul National University. His research interests include the design and control of underactuated tendon-driven robot and robotic hand.

Dongjun Lee (S'02-M'04) is an Associate Professor with the Department of Mechanical & Aerospace Engineering at the Seoul National University. He received the B.S. and M.S. degrees from KAIST, Korea, and the Ph.D. degree in mechanical engineering from the University of Minnesota, respectively in 1995, 1997 and 2004. He was an Assistant Professor with the Department of Mechanical, Aerospace & Biomedical Engineering at the University of Tennessee, 2006-2011, and a Postdoctoral Researcher with the Coordinated Science Laboratory at the University of Illinois at Urbana-Champaign, 2004-2006. His main research interests are dynamics and control of robotic and mechatronic systems with emphasis on teleoperation/haptics, multirobot systems, aerial robots, and geometric mechanics control theory. Dr. Lee received the US NSF CAREER Award in 2009, the Best Paper Award from the IAS-2012, and the 2002-2003 Doctoral Dissertation Fellowship of the University of Minnesota. He was an Associate Editor of the IEEE Transactions on Robotics, and an Editor for the IEEE International Conference on Robotics & Automation 2015-2017.